Molecular Therapy
Nucleic Acids
Original Article

Long noncoding RNA *Cfast* regulates cardiac fibrosis

Feng Zhang,[1,2,8] Xuyang Fu,[1,2,8] Masaharu Kataoka,[3,9] Ning Liu,[1,2] Yingchao Wang,[4] Feng Gao,[1,2] Tian Liang,[1,2] Xiaoxuan Dong,[1,2] Jianqiu Pei,[5] Xiaoyun Hu,[3] Wei Zhu,[1] Hong Yu,[1] Douglas B. Cowan,[3] Xinyang Hu,[1] Zhan-Peng Huang,[6] Jian'an Wang,[1] Da-Zhi Wang,[3,7] and Jinghai Chen[1,2]

[1]Department of Cardiology, Provincial Key Lab of Cardiovascular Research, Second Affiliated Hospital, Zhejiang University School of Medicine, Hangzhou 310009, China; [2]Institute of Translational Medicine, Zhejiang University School of Medicine, Hangzhou 310029, China; [3]Department of Cardiology, Boston Children's Hospital, Harvard Medical School, 300 Longwood Avenue, Boston, MA 02115, USA; [4]Pharmaceutical Informatics Institute, College of Pharmaceutical Sciences, Zhejiang University, Hangzhou 310058, China; [5]State Key Laboratory of Cardiovascular Disease, Fuwai Hospital, National Center for Cardiovascular Disease, Chinese Academy of Medical Sciences and Peking Union Medical College, Beijing 100037, China; [6]Department of Cardiology, Center for Translational Medicine, Institute of Precision Medicine, The First Affiliated Hospital, Sun Yat-sen University, Guangzhou, China; [7]Harvard Stem Cell Institute, Harvard University, Cambridge, MA 02138, USA

Cardiac fibrosis occurs in most cardiac diseases, which reduces cardiac muscle compliance, impairs both systolic and diastolic heart function and, ultimately, leads to heart failure. Long noncoding RNAs (lncRNAs) have recently emerged as important regulators of a variety of biological processes; however, little is known about the expression and function of lncRNAs in cardiac fibrosis. Using unbiased transcriptome profiling in a mouse model of myocardial infarction (MI), we identified a cardiac fibroblast-enriched lncRNA (AK048087) named cardiac fibroblast-associated transcript (*Cfast*), which is significantly elevated after MI. Silencing *Cfast* expression by small interfering RNAs (siRNAs) or lentiviral short hairpin RNAs (shRNAs) resulted in suppression of fibrosis-related gene expression and transdifferentiation of myofibroblasts into cardiac fibroblasts. Depletion of *Cfast* by lentiviral shRNAs in mouse hearts significantly attenuated cardiac fibrosis induced by MI or isoproterenol-infusion. Importantly, inhibition of *Cfast* ameliorated cardiac function following cardiac injury. RNA pull-down followed by mass spectrometry analyses identified COTL1 (coactosin-like 1) as one of the *Cfast* interacting proteins. Mechanistically, *Cfast* competitively inhibits the COTL1 interaction with TRAP1 (transforming growth factor-β receptor-associated protein 1), which enhances TGF-β signaling by augmenting SMAD2/SMAD4 complex formation. Therefore, our study identifies *Cfast* as a novel cardiac fibroblast-enriched lncRNA that regulates cardiac fibroblast activation in response to pathophysiological stress. *Cfast* could serve as a potential therapeutic target for the prevention of cardiac fibrosis and cardiac diseases.

INTRODUCTION

Cardiovascular diseases remain a major cause of health loss and cost in the world.[1] As a common pathophysiologic companion, cardiac fibrosis occurs in most heart diseases, impacting both systolic and diastolic function.[2,3] Cardiac fibroblasts (CFs) exert essential roles in fibrotic responses following acute and chronic stress resulting from myocardial infarction (MI), hypertension, scar formation, and tissue repair.[4,5] Under pathological conditions, CFs proliferate and transdifferentiate into myofibroblasts, which are characterized by the expression of α-smooth muscle actin (ACTA2) and are responsible for the production of excessive extracellular matrix (ECM) and the formation of a collagen-rich fibrotic scar.[5,6] The progressive interstitial fibrosis and fibrotic scar accumulates throughout the myocardium, resulting in a reduction of cardiac muscle compliance, impairment of cardiac function, and, eventually, heart failure.[3–5] Despite the appreciation of the importance of pathological remodeling in heart diseases, there is still a lack of effective therapies directly targeting CF responses and fibrotic remodeling. In addition, the molecular mechanisms underlying fibrosis-associated heart diseases remain unclear.

It is now widely recognized that the majority of the mammalian genome is actively transcribed to RNA. A small part of the RNAs are protein-coding transcripts, while the majority of these transcribed RNAs constitute non-coding RNA, including a large number of long noncoding RNAs (lncRNAs), which are more than 200-nucleotides in length. Emerging evidence suggests that lncRNAs play important roles in diverse biological processes and diseases.[7,8] In particular, recent studies have reported the function of lncRNAs are associated with a variety of cardiovascular disease responses,[9,10] including the

Received 10 August 2020; accepted 18 November 2020;
https://doi.org/10.1016/j.omtn.2020.11.013.

[8]These authors contributed equally

[9]Present address: Department of Cardiology, Keio University School of Medicine, Shinanomachi 35, Shinjuku-ku, Tokyo 160-8582, Japan

Correspondence: Da-Zhi Wang, PhD, Department of Cardiology, Boston Children's Hospital, Harvard Medical School, 300 Longwood Avenue, Boston, MA 02115, USA.
E-mail: dwang@enders.tch.harvard.edu
Correspondence: Jinghai Chen, PhD, Department of Cardiology, Provincial Key Lab of Cardiovascular Research, Second Affiliated Hospital, Zhejiang University School of Medicine, Hangzhou 310009, China.
E-mail: jinghaichen@zju.edu.cn

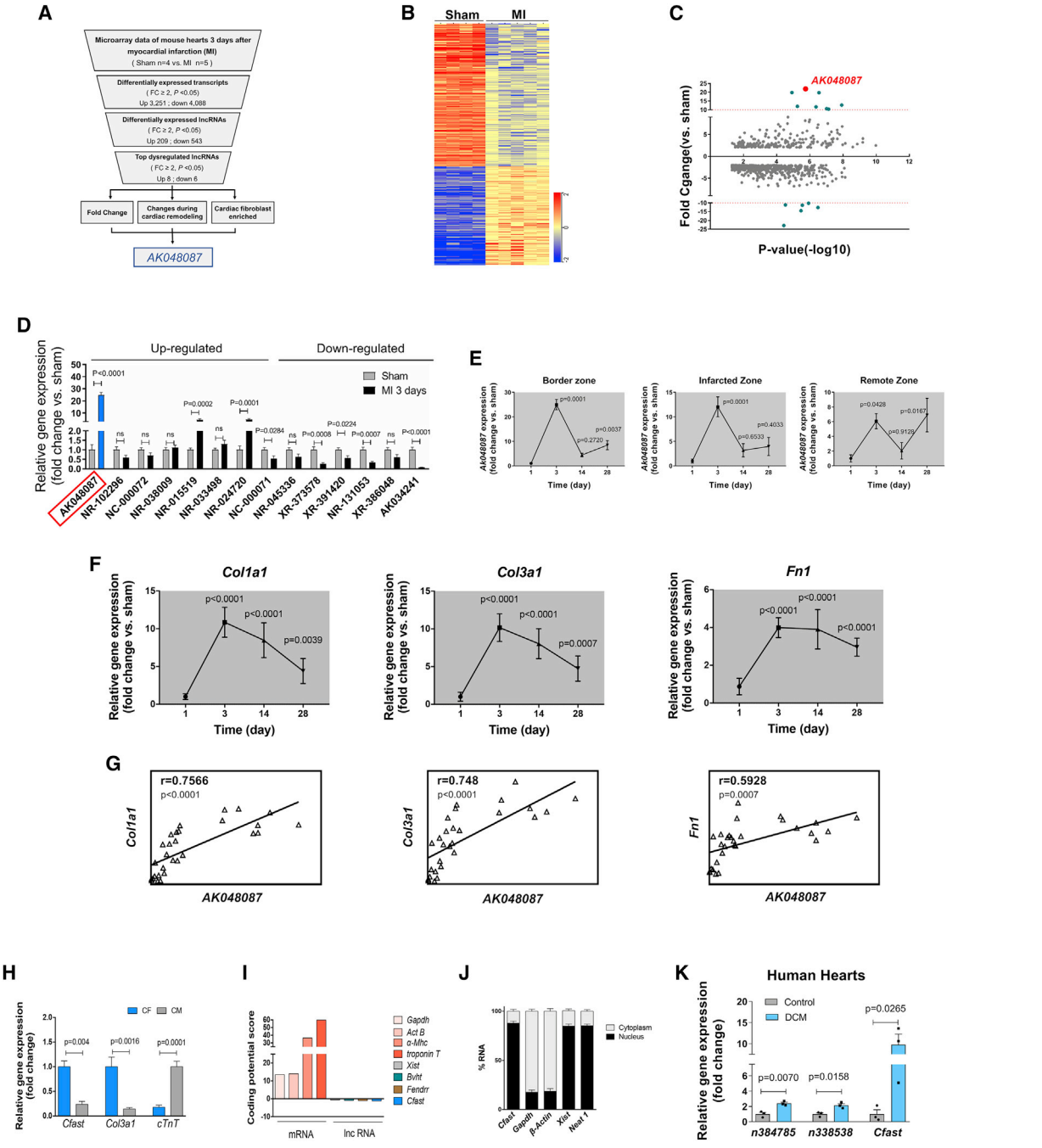

Figure 1. *Cfast* is a cardiac fibroblast-enriched lncRNA upregulated in the heart after MI

(A) Workflow of discovery of lncRNAs in mouse model of MI. (B) Heatmap of differentially expressed lncRNAs in the heart 3 days after MI (n = 5) versus sham (n = 4; microarray FC ≤ 0.5 or ≥ 2, unpaired t test p value ≤ 0.05). (C) Enrichment plot of *Cfast* and dysregulated lncRNAs in the heart 3 days after MI. The x axis shows p value and the y axis shows lncRNAs fold change versus sham. (D) qRT-PCR of top up- and downregulated lncRNAs in the heart 3 days after MI. *AK048087* is highlighted in blue. Graphs show means normalized to sham ± SEM (n = 6 to 8 animals per group). p values were determined by Student's t test. (E) qRT-PCR of *Cfast* expression in the border zone (left panel), infarct zone (middle panel), and remote zone (right panel) of infarcted hearts at 3, 14, and 28 days. Graphs show means normalized to sham ± SEM (n = 6 to 8 animals per group). p values were determined by one-way ANOVA. (F) Time course of ECM relative gene expression after MI. Graphs show means normalized to sham ± SEM (n = 6 to 8 animals). p values were determined by one-way ANOVA (Dunnett's multiple comparisons test). (G) Positive correlation of *Cfast* expression and fibrosis genes. Pearson's correlation test (r; 95% confidence interval [CI]). (H) qRT-PCR of *Cfast* expression in cardiomyocytes and cardio-fibroblasts. Data show mean ± SEM (n ≥ 4). p values are determined by Student's t test. (I) Coding potential of *Cfast*. Protein coding mRNAs and known non-coding lncRNAs serve as positive and negative controls, respectively.

(legend continued on next page)

regulation of atherosclerosis and plaque inflammation,[11] modulation of cardiac hypertrophy,[12–15] and cardiomyocyte proliferation and cardiac regeneration.[16–19] We have previously found that long intergenic noncoding RNA (lincRNA)-p21 plays a critical role in cell proliferation and neointimal formation during cardiovascular remodeling.[20] More recently, we reported that many lncRNAs are dynamically expressed in ischemic cardiomyopathy (ICM) and these lncRNAs regulate the expression and function of the ECM and cardiac fibrosis during the development of ICM.[21] Several lncRNAs, like *Wisper*, *Meg3*, and *Safe*, have been demonstrated as powerful regulators of cardiac fibrosis.[22–24] At the same time, the significance of lncRNAs in regulating cardiac fibrosis and their underlying molecular mechanisms have yet to be fully addressed.

To gain insight into fibrosis-related lncRNAs in the heart, we performed unbiased screening using a mouse model of MI and detected 752 differentially expressed lncRNAs in the infarcted heart. We identified a novel cardiac fibroblast-enriched lncRNA, named cardiac fibroblast-associated transcript (*Cfast*), and found that it modulates cardiac fibrosis upon acute and chronic cardiac injury. We showed that *Cfast* participates in the regulation of the transforming growth factor-β (TGF-β) signaling pathway by interacting with COTL1 (coactosin-like 1). Inhibition of *Cfast* during and/or after cardiac injury effectively prevents pathological fibrotic remodeling and improves heart function in a mouse model of MI. As a result, our study identifies a fibroblast-enriched lncRNA, which may represent a novel regulator and potential therapeutic target for cardiac fibrotic remodeling in cardiac disorders.

RESULTS

Cfast is a cardiac fibroblast-enriched lncRNA upregulated in the heart after MI

To explore the key lncRNAs involved in regulating essential pathophysiological processes of the adult heart, we performed microarray-based transcriptome profiling on mouse hearts 3 days after MI or sham surgery (Figure 1A). Microarray analysis revealed a total of 7,339 differentially expressed transcripts in MI hearts compared to sham controls (fold change [FC] $\geq$ 2, $p < 0.05$; Figure 1B). Kyoto Encyclopedia of Genes and Genomes (KEGG) or Gene Ontology (GO) pathway analyses revealed that oxidative phosphorylation, ECM-receptor interaction, cell proliferation, and inflammatory responses were among the top dysregulated genes in MI hearts (Figures S1A and S1B), consistent with prior reports.[4,25] Interestingly, 209 lncRNAs are upregulated and 543 lncRNAs are downregulated in MI hearts (FC $\geq$ 2, $p < 0.05$; Figure 1C). Among these lncRNA transcripts, we found that 8 lncRNAs are mostly upregulated and 6 lncRNAs mostly downregulated (FC $\geq$ 2, $p < 0.05$), whereas the expression level of the AK048087 transcript was increased by 25-fold (Figure 1D). Interestingly, lncRNA AK034241 appears to be the most downregulated lncRNA (Figures 1C and 1D), which will be reported in a separate study.

To confirm the above results and identify top lncRNA candidates for further study, we performed an independent series of mouse heart infarctions (sham n = 8 versus MI n = 7). We examined the expression, using qRT-PCR, of the top up- and downregulated lncRNAs identified from the above microarray screening in MI hearts and we verified that AK048087 expression increased the most in the hearts 3 days after MI. To better characterize the expression of this lncRNA during cardiac remodeling in response to MI, we carefully examined its expression in the heart 3, 14, and 28 days after MI. In particular, we examined its expression in the MI border zone, infarct zone, and remote zone. Substantially increased expression of lncRNA AK048087 was observed in all zones of the heart 3 days after MI (Figure 1E), which diminished by 14 and 28 days. Cardiac remodeling after MI is associated with the formation of scar and the expression of fibrosis-related genes.[22] Therefore, we tested the expression of *Col1a1*, *Col3a1*, and *Fibronectin (Fn1)* and found their expression increased in the MI hearts (Figure 1F). Interestingly, the expression pattern of these fibroblast-related genes is closely correlated with that of lncRNA AK048087 in infarcted hearts (Figure 1G).

Given its increased expression and positive correlation with that of fibrosis-related genes in infarcted hearts, we decided to focus on lncRNA AK048087 and renamed it *Cfast*. To investigate cell type distribution of *Cfast* in the heart, we dissociated the cardiomyocytes (CMs) and CFs of adult mouse hearts. qRT-PCR profiling showed that the *Cfast* transcript is enriched in CFs. As positive controls, we show that *Col3a1* is enriched in CFs, while *cTnT* is enriched in CMs (Figure 1H). The gene encoding *Cfast* is located on mouse chromosome 4 and appears to produce a single exon transcript (Figure S2A). *Cfast* is highly conserved in both DNA sequence and its genome locus across multiple species (Figure S2B). In addition to the heart, *Cfast* expression is also detected in other mouse tissues (Figure S2C). We performed 3′ and 5′ rapid amplification of cDNA end (RACE) assays, using RNAs isolated from adult mouse hearts and we obtained the full-length *Cfast* transcript of 2,418 nt (Figures S3A and S3B). To test whether *Cfast*, which contains several putative open reading frames (ORFs), is a noncoding RNA, we employed the Protein Coding Potential Calculator[26] to evaluate the protein-coding potential of full-length *Cfast* transcript. As expected, *Cfast* has low coding-potential score, similar to that of well-studied lncRNAs *Xist*, *Bvht*, and *Fendrr*. In contrast, protein-coding genes, like *Gapdh*, *Act-B*, *α-Mhc*, and *troponin T*, all exhibit high coding potential scores (Figure 1I).

Next, we asked whether *Cfast* has the potential to encode micro-peptides. Using mass spectrometry assays at the detecting sensitivity of 10 pg, we were unable to detect any predicted micro-peptides from adult hearts, suggesting *Cfast* is unlikely to encode micro-peptides (Figure S3C). Finally, we performed subcellular fractionation assays to determine the subcellular location of *Cfast* transcripts. qRT-PCR assays

(J) *Cfast* is enriched in nucleus of cardio-fibroblasts. Percentage of nuclear (black bar) and cytoplasmic (gray bar) RNA concentrations of *Cfast*, *Gapdh*, and *β-actin* (cytoplasmic markers), and *Neat1* and *Xist* (nuclear markers) measured by qRT-PCR after subcellular fractionation in CFs. Data represent mean ± SEM (n = 3). (K) qRT-PCR of *Cfast* expression in human heart samples from dilated cardiomyopathy (DCM) patients and controls. Data show mean ± SEM (n = 3). p values were determined by Student's t test.

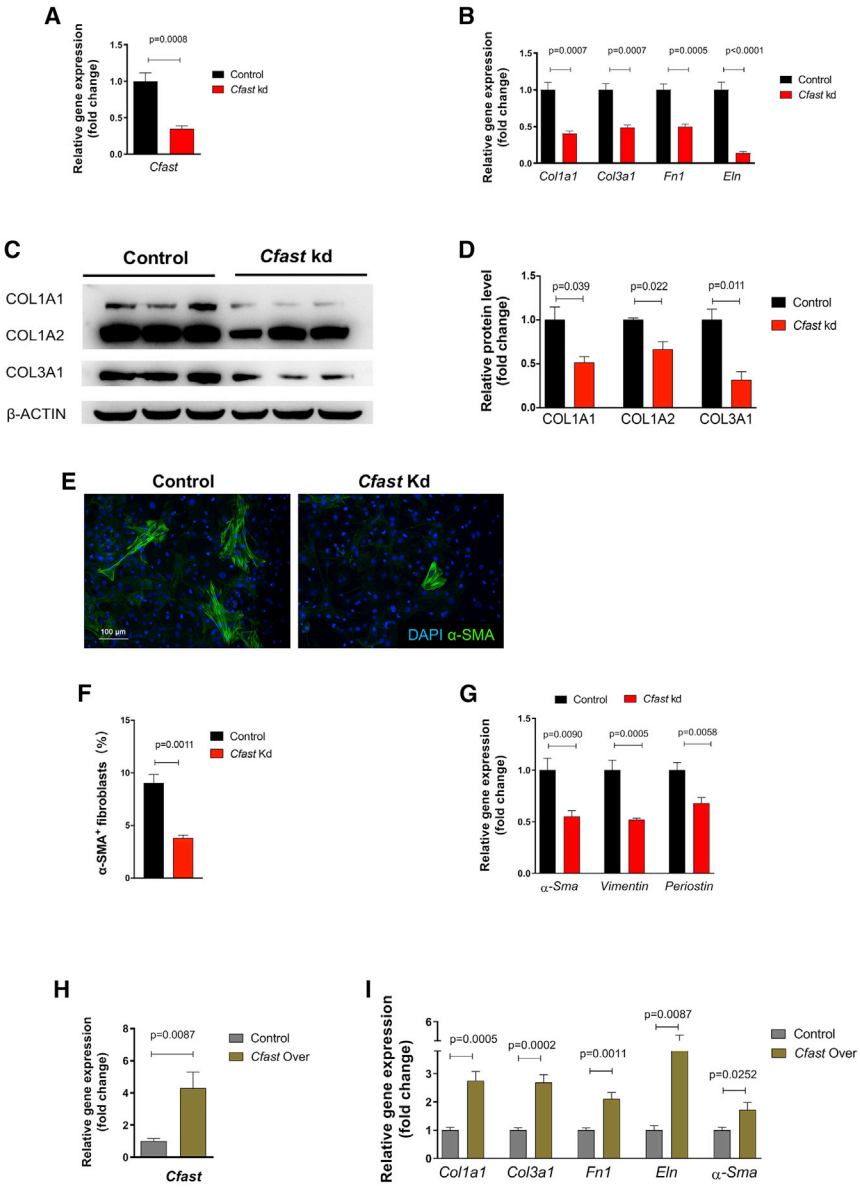

Figure 2. Knockdown of *Cfast* inhibits myofibroblast differentiation in isolated cardiac fibroblasts

(A) Expression of *Cfast* after lentivirus-based knockdown in cardiac fibroblasts. Data represent mean ± SEM (n = 6); p values were determined by Student's t test. (B) Reduced expression of fibrosis genes after *Cfast* knockdown (Kd) in cardiac fibroblasts. Data represent mean ± SEM (n = 6), p values were determined by Student's t test. (C) Western blot showing the expression of indicated protein in control and *Cfast* kd fibroblasts. (D) Quantification of western blot band density. n = 3. p values were determined by Student's t test. (E) Immunostaining of α-smooth muscle actin (α-SMA) in control and *Cfast* kd fibroblasts. α-SMA labels activating cardiac fibroblasts (green) and DAPI labels nuclei (blue). (F) Quantification of α-SMA positive cells in control and *Cfast* kd fibroblasts. p values were determined by Student's t test. (G) qRT-PCR of the expression of *α-Sma*, *Vimentin*, and *Periostin* genes in control and *Cfast* kd fibroblasts. p values were determined by Student's t test. (H and I) Mouse cardiac fibroblasts were transfected with lentivirus-*Cfast* to overexpress *Cfast* (*Cfast* Over) or with lentivirus-GFP (control) for 48 h. Gene expression of *Cfast* (H) and fibrosis related genes (I), Col1a1, Col3a1, Fn1, Eln, and α-SMA were measured by qRT-PCR. Data represent mean ± SEM (n = 6). p values were determined by Student's t test.

revealed that the *Cfast* transcript is predominantly in the nuclear fraction of cardiac fibroblasts, similar to the previously identified lncRNAs *Xist* and *Neat1* (Figure 1J). To assess the clinical relevance of our findings, we studied the expression of the *Cfast* human homolog and confirmed its expression as the previous reported human lncRNAs n384785 and n338538.[21] Expression of *Cfast* was significantly increased in patients with dilated cardiomyopathy (DCM) (Figure 1K)

Knockdown of *Cfast* inhibits myofibroblast differentiation in isolated cardiac fibroblasts

To determine the function of *Cfast*, we employed a loss-of-function approach to assess the effect of downregulation of *Cfast* in cardiac fibroblasts isolated from neonatal mouse hearts. Using a lentivirus-based knockdown approach to specifically target *Cfast*, we consistently achieved more than 60% knockdown of *Cfast* levels (Figure 2A). qRT-PCR revealed a significant downregulation of the expression of fibrotic related genes *Col1a1*, *Col3a1*, *fibronectin (Fn1)*, and *elastin (Eln)* when *Cfast* is knocked down (Figure 2B). Similarly, we observed that protein levels of Col1A1, Col1A2, and Col3A1 were reduced in *Cfast* knockdown cells (Figures 2C and 2D). Next, we performed immunofluorescence staining of α-smooth muscle actin (α-SMA) as a marker of myofibroblast transdifferentiation. We observed less α-SMA positive cells upon *Cfast* silencing (Figure 2E) and quantification confirmed this observation (Figure 2F). Furthermore, we found that the transcript level of *α-Sma* was reduced when *Cfast* is diminished (Figure 2G). In addition, the expression of *Vimentin* and *Periostin*, which are molecular markers of fibroblast activation, was reduced (Figure 2G).

We applied an independent small interfering RNAs (siRNA) that targets a distinct site of the *Cfast* gene in isolated mouse CFs and confirmed that the abovementioned fibrosis-related genes, *Col1a1*, *Col3a1*, *Fn1*, *Eln*, and *α-Sma*, are all markedly downregulated (Figure S4A). Conversely, we found that overexpression of *Cfast* by lentivirus (Figure 2H) resulted in significant upregulation in the fibrosis-related genes *Col1a1*, *Col3a1*, *Fn1*, *Eln*, and *α-Sma* (Figure 2I) in cardiac fibroblasts. Together, these findings indicate that *Cfast* regulates the expression fibrotic genes and the differentiation of cardiac fibroblasts.

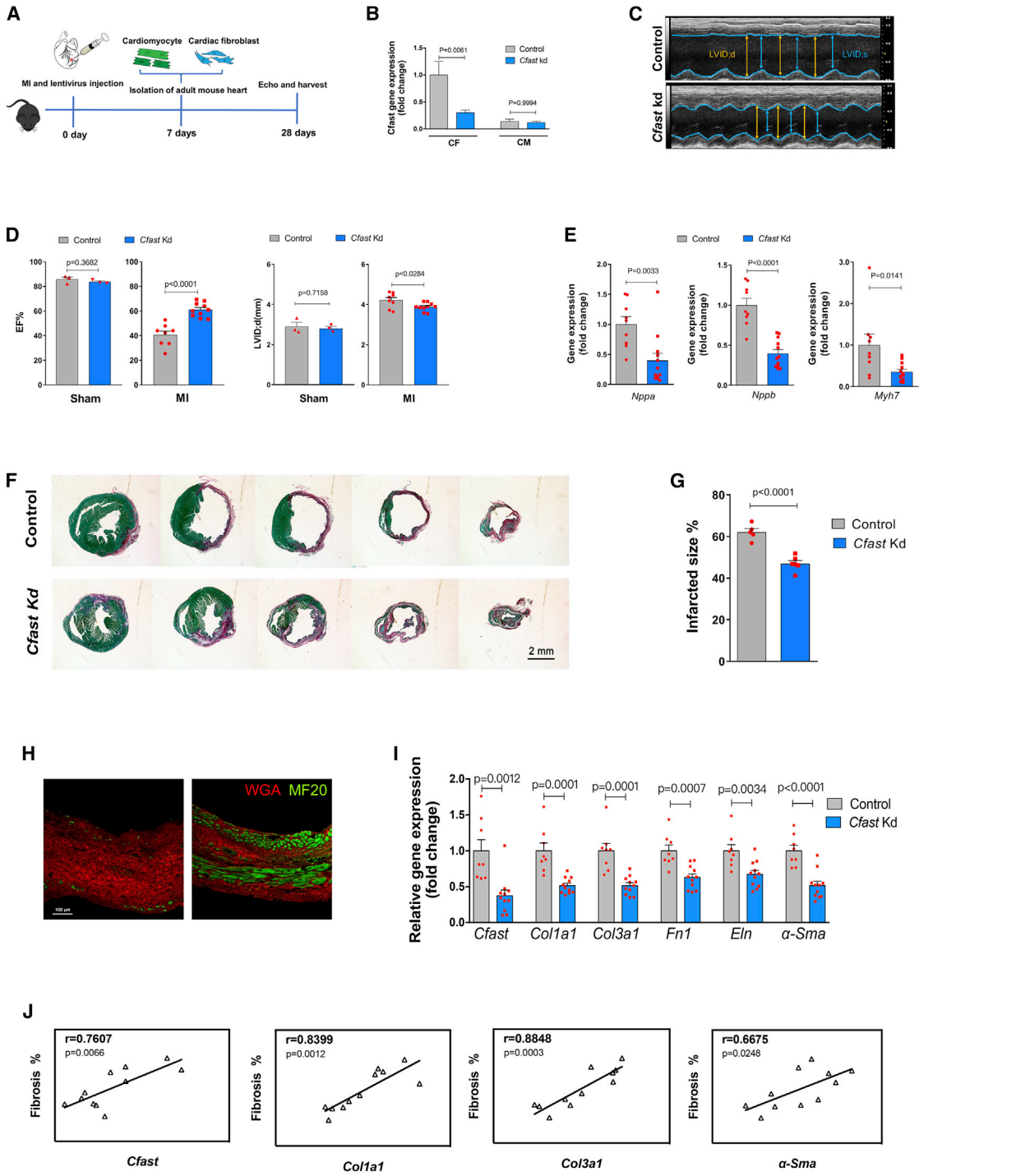

Figure 3. Inhibition of *Cfast* reduces scar size and improves cardiac function in response to MI

(A) Workflow of testing *Cfast* function during MI. (B) qRT-PCR of *Cfast* in isolated cardiomyocytes and fibroblasts 7 days after cardiac-injection of *Cfast* depletion lentivirus and MI. Data are mean fold change relative to sham ± SEM (n = 3). p values versus sham determined by two-way ANOVA Tukey's test. (C) M-mode echocardiography of mice 28 days after cardiac-injection of *Cfast* depletion lentivirus and MI. (D) Measurement of cardiac function of mice by echocardiography 28 days after cardiac injection of *Cfast* depletion lentivirus and control lentivirus subjected to MI or sham. Graphs show mean values ± SEM. Sham treatment: control n = 3 versus *Cfast* Kd n = 3. MI treatment: control n = 8, *Cfast* Kd n = 10. p values were calculated by Student's t test. (E) qRT-PCR of cardiomyopathy marker genes of mouse hearts 28 days after cardiac-injection of *Cfast* depletion lentivirus and MI. Bars represent means normalized to control ± SEM ($n \geq 8$). p values were determined by Student's t test. (F) Representative images of series

(legend continued on next page)

Inhibition of *Cfast* reduces scar size and improves cardiac function in response to MI

Given its anti-fibrotic effects in cultured cardiac fibroblasts, we tested the therapeutic potential of *Cfast* inhibition in mouse hearts in response to MI. The left anterior descending coronary artery was permanently ligated to create MI and a *Cfast*-depletion lentivirus was directly injected into the myocardium at regions adjacent to the ligation site. Cardiac function and the development of fibrosis was analyzed after 28 days (Figure 3A). We first determined the cell-type specificity and knockdown efficiency 7 days after MI and *Cfast*-depletion lentivirus injection. Indeed, we found that *Cfast* expression was significantly downregulated in the isolated adult cardiac fibroblast fraction, but not in the adult cardiomyocyte fraction, indicating that lentivirus knockdown of *Cfast* is specifically effective in cardiac fibroblasts opposed to cardiomyocytes (Figure 3B). This observation was not due to the isolation process because both cardiomyocyte and fibroblast-specific marker genes were detected and confirmed in the respective isolated cells (Figures S5A and S5B).

28 days after MI and *Cfast* inhibition, cardiac dimensions, and function were measured using echocardiography. We found that mice with *Cfast* depletion exhibited improved cardiac function, as evidenced by preserved ejection fraction (EF%), with prevention of cardiac dilation (LVID;d(mm)), when compared to the control group. In the absence of MI injury (sham), *Cfast* inhibition did not impact cardiac function compared to the control group. (Figures 3C and 3D; Table S1). Furthermore, the heart weight to bodyweight ratio is substantially lower in *Cfast*-depleted hearts (Figure S6A). Molecular marker analysis demonstrated significant reduction of the expression of cardiomyopathy marker genes such as *Nppa*, *Nppb*, and *Mhy7* in the heart after *Cfast* inhibition and MI (Figure 3E). This further supports the view that inhibition of *Cfast* ameliorates cardiac function after MI. Interestingly, we found decreased cardiomyocyte size in *Cfast* depleted hearts (Figure S6B).

We next assessed whether *Cfast* inhibition prevents cardiac fibrosis and pathological remodeling. Histological analyses revealed that *Cfast* inhibition reduced scar formation in infarcted hearts (Figures 3F and 3G). Interestingly, immunohistochemical analysis showed that more MF20-positive cardiomyocytes exist in the scar regions of *Cfast* knockdown hearts when compared with that of control hearts (Figure 3H). Consistent with the above observation, we found that the expression levels of fibrosis-related genes, *Col1a1*, *Col3a1*, *Fn1*, *Eln*, and *α-Sma* are all markedly reduced in *Cfast* knockdown hearts after MI (Figure 3I). In support of these results, we found that post-infarction fibrosis is positively correlated with *Cfast* expression, as well as the fibrosis-associated genes, *Col1a1*, *Col3a1*, and *α-Sma* (Figure 3J); yet, suppression of fibrotic gene expression was not observed in the sham treatment (Figure S7).

Given that *Cfast* inhibition resulted in the reduction of cardiomyocyte size in the heart (Figures S6A and 6B), while *Cfast* is predominately expressed in cardiac fibroblasts, we set out to test the hypothesis that cardiac fibroblast-expressed *Cfast* represses cardiomyocyte hypertrophic growth via a paracrine mechanism. Cultured neonatal mouse cardiomyocytes were treated with conditioned media from cultured cardiac fibroblasts transfected with Control or *Cfast* knockdown lentivirus (Figure S6C). We found cardiomyocyte size was substantial reduced after treatment with *Cfast* knockdown conditioned medium (Figure S6D). These results suggest a paracrine mechanism where *Cfast* silencing in fibroblasts affects cardiomyocyte responses.

Collectively, our results demonstrate that *Cfast* plays an important role in pathological cardiac fibrosis and remodeling in response to MI.

Cfast depletion blocks isoproterenol-induced cardiac fibrosis in mouse hearts

The above results, in which inhibition of *Cfast* in the heart reduced scar formation and affected remodeling of cardiomyocytes in response to MI, prompted us to more specifically investigate the role of *Cfast* in regulating cardiac fibrosis during remodeling. We decided to employ a chronic cardiac pathological model by daily injection of isoproterenol (ISO, 30 mg/kg) for 21 days in mice—an experimental procedure that has been well-documented to induce cardiac fibrosis and impair cardiac function.[27] At day 8, we injected lentivirus to silence *Cfast*, while a scrambled sequence was used as a control (Figure 4A). We assessed cardiac phenotypes at 21 days and found that ISO injection resulted in a reduction of cardiac function and *Cfast*-depletion in these hearts significantly improved cardiac function compared to controls (Figure 4B; Table S2). Improved cardiac function in these hearts is supported by a reduction in the expression of cardiomyopathy molecular marker genes, including *Nppa*, *Nppb*, and *Myh7* (Figure 4C).

Histological examination using Sirius Red and Fast Green staining to assess fibrosis indicates that *Cfast*-depletion markedly prevented ISO-induced cardiac pathological fibrosis (Figure 4D), which was confirmed by quantification (Figure 4E). The above observation was further confirmed by the analysis of collagen content with polarized light, where we found a dramatic reduction of collagen in *Cfast*-inhibited hearts (Figure 4F). Finally, we found the expression

of transverse sections of mouse hearts 28 days after cardiac injection of *Cfast* depletion lentivirus and MI. Sirius red/fast green collagen staining marks myocardium (green) and scar (red). Scale bar, 2 mm. (G) Quantification of the size of scar. (Control n = 5, *Cfast* Kd n = 6). p values were calculated by Student's t test. (H) Immunohistochemistry of left ventricle of mouse hearts 28 days after cardiac injection of *Cfast* depletion lentivirus and MI. Wheat germ agglutinin (WGA) marks fibrotic area (red) and MF20 labels myocardium (green). (I) qRT-PCR of *Cfast* and fibrosis genes of mouse hearts 28 days after cardiac-injection of *Cfast* depletion lentivirus and MI. (control n = 8, *Cfast* Kd n = 10) p values were calculated by Student's t test. (J) Positive correlation of *Cfast* expression and fibrosis genes in mouse hearts 28 days after cardiac injection of *Cfast* depletion lentivirus and MI. Pearson's correlation test (r; 95% CI).

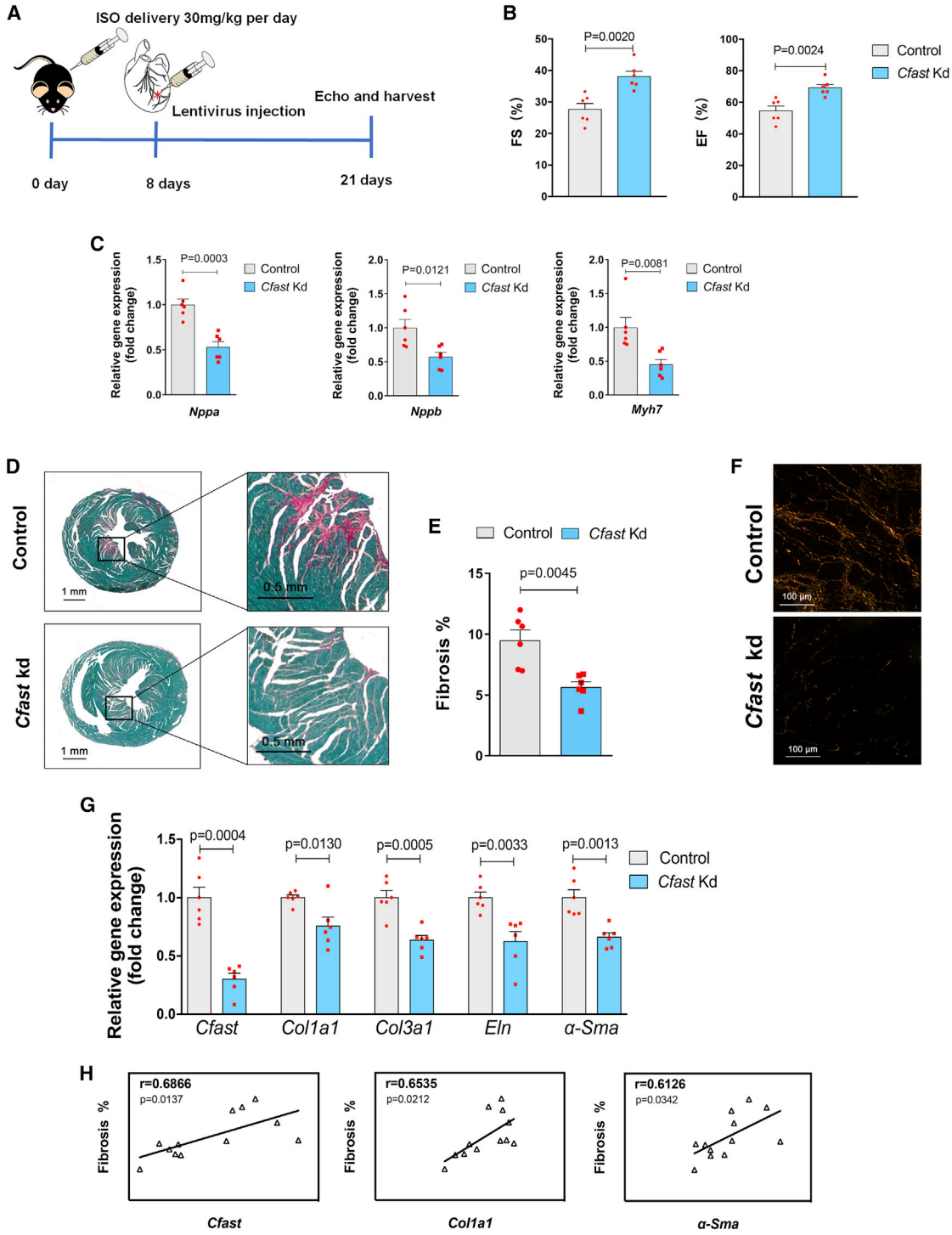

Figure 4. *Cfast* depletion blocks ISO-induced cardiac fibrosis in mouse hearts

(A) Workflow of testing *Cfast* function in ISO-induced cardiac fibrosis and heart failure. (B) Measurement of cardiac function by echocardiography 21 days after cardiac injection of *Cfast* depletion lentivirus and ISO-infusion. Graphs show mean values normalized to the average value of the control group ± SEM (control n = 6, *Cfast* Kd n = 6); p values were calculated by Student's t test. (C) qRT-PCR of cardiomyopathy marker genes of mouse hearts 21 days after cardiac injection of *Cfast* depletion lentivirus and ISO-infusion. Bars represent means normalized to control ± SEM (n = 6). p values were determined by Student's t test. (D) Representative images of series of transverse sections of mouse hearts 21 days after cardiac injection of *Cfast* depletion lentivirus and ISO-infusion. Sirius red/fast green collagen staining marks myocardium (green) and

(legend continued on next page)

of cardiac fibrosis-associated genes, *Col1a1*, *Col3a1*, *Eln*, and *α-Sma*, was repressed by *Cfast* depletion (Figure 4G). In line with the role of *Cfast* in the regulation of cardiac fibrosis, we found that ISO-induced fibrosis is correlated with the expression of *Cfast* and cardiac fibrosis-related genes *Col1a1* and *α-Sma* (Figure 4H). Furthermore, the heart weight to body weight ratio is substantially lower in *Cfast*-depleted hearts (Figure S8A). Consistent with the view that *Cfast* inhibition prevents cardiac hypertrophic growth, we found reduced cardiomyocyte size in *Cfast*-depleted hearts (Figure S8B). Together, these results establish an important role of *Cfast* in the development of cardiac fibrosis, cardiac remodeling, and function.

Cfast is an important regulator of the fibrosis program

To better understand how loss of *Cfast* affects gene expression in cardiac fibroblasts, we performed RNA sequencing (RNA-seq) using *Cfast* knockdown CFs. We identified 3,951 differentially expressed genes (log2 FC > 0.5; $p < 0.05$) in *Cfast*-knockdown compared to control CFs, of which 1,880 genes were upregulated and 2,071 downregulated (Figure 5A). GO term enrichment analysis revealed that downregulated genes primarily related to "cell differentiation, cell migration, extracellular matrix organization, response to TGF-β, and cell proliferation," are among the most enriched terms (Figure 5B). Similarly, KEGG pathway analysis indicated that ECM-receptor interaction and focal adhesion, which are linked to fibrosis, are among the most affected pathways in *Cfast*-silenced CFs (Figure 5C). We subsequently examined genes related to ECM organization in detail.

Using gene set enrichment (GSE) analysis, we found that "extracellular matrix organization," including "ECM proteoglycans, collagen formation, and non-integrin membrane ECM interactions" were dramatically downregulated in *Cfast*-knockdown CFs (Figure 5D). In addition to the downregulation of ECM genes (e.g., *Col4a3* and *Col4a4*) closely-associated with fibrosis in *Cfast*-knockdown CFs, we observed that genes related to cell proliferation (e.g., *Mmp2* and *Sox4*), cell migration (e.g., *Tgfbr1* and *Tgfbr3*), and cell differentiation (e.g., *Akap6* and *Cap2*) are also downregulated in *Cfast*-knockdown CFs (Figure 5E). This decreased expression of fibrosis-related genes in *Cfast*-knockdown CFs is consistent with the reduced cardiac fibrosis observed in MI- and ISO-stimulated hearts *in vivo*. Together, these results support the view that *Cfast* plays an important role in fibrotic gene expression and cardiac fibrosis processes during cardiac remodeling in response to pathophysiological stress.

Cfast is associated with COTL1 protein to regulate the TGF-β signaling pathway

To elucidate the molecular mechanism by which lncRNA *Cfast* modulates cardiac fibrosis, we attempted to identify *Cfast*-interacting proteins. We performed RNA pull-down assays by labeling full-length *Cfast* RNA with biotin and mixing it with cellular lysates of cardiac fibroblasts. Putative *Cfast* binding proteins were then identified by mass spectrometry. Using the criteria of unique sequence coverage and fold enrichment, we identified five proteins that potentially interact with *Cfast* (Figure 6A). These include ABCF1 (ATP-binding cassette, sub-family F [GCN20], member 1), AIMP2 (aminoacyl tRNA synthetase complex-interacting multifunctional protein 2), S100A11 (S100 calcium binding protein A11), COTL1, and STAU1 (staufen double-stranded RNA binding protein 1).

Previous studies showed that ABCF1 functions as a regulator of immune responses,[28,29] AIMP2 plays roles in cancer development[30] and Parkinson's disease,[31,32] S100A11 is required for efficient plasma membrane repair,[33] and STAU1 promotes cell survival.[34,35] Therefore, none of these proteins appear functionally relevant with the cardiac fibrotic phenotype. Interestingly, COTL1 was reported to be involved in TGF-β signaling[36] and inhibit neuronal migration during mouse corticogenesis,[37] suggesting that COTL1 could be a *Cfast* binding protein to regulate cardiac fibrosis. To confirm the mass spectrometry data, we performed a *Cfast* RNA pull-down assay coupled with western blotting to detect COTL1 after the lncRNA *Cfast* pull-down. The binding of COTL1 was readily detected in the *Cfast* pull-down sample but not in the control (Figure 6B). The association of COTL1 with *Cfast* was independently confirmed by RNA immunoprecipitation (RIP). Using qRT-PCR, we found that *Cfast* transcripts were associated with the COTL1 immunoprecipitants, but not that of control IgG samples (Figure 6C). The *Cfast*-COTL1 interaction is specific, since knockdown of *Cfast* abolished COTL1-associated *Cfast* RNA (Figure 6C).

A previous study using a yeast two-hybrid screen identified that 5-lipoxygenase (5LO) interacts with COTL1, and that 5LO also interacts with TRAP1,[38] which is a SMAD4 chaperone involved in TGF-β signaling by facilitating the interaction of SMAD4 with SMAD2.[39] It is tempting to speculate that COTL1 could associate with TRAP1 to mediate the downstream signaling. Therefore, the identification of the interaction between *Cfast* and COTL1 prompted us to test the hypothesis that lncRNA *Cfast* and its interaction with COTL1 will competitively abrogate the interaction between COTL1 and TRAP1, leading to an interaction between TRAP1 and SMAD4; thus, increasing formation of the SMAD2/4 complex. As a result, the TGF-β/SMAD-mediated fibrotic signal would be enhanced. If this hypothesis is correct, we would predict that *Cfast* will enhance TGF-β signaling and increase fibrosis. Conversely, silencing or knockdown *Cfast* could diminish TGF-β signaling and fibrosis.

scar (red). Scale bars, 1 mm. (E) Quantification of the size of scar. (Control n = 5, *Cfast* Kd n = 4). p values were calculated by Student's t test. (F) Representative images of Sirius red/fast green collagen staining. Sections were visualized under polarized light microscopy. Collagen type I is shown in yellow orange. Collagen type III is shown in green. Scale bars, 100 μM. (G) qRT-PCR of *Cfast* and fibrosis genes of mouse hearts 21 days after cardiac injection of *Cfast* depletion lentivirus and ISO-infusion. (Control n = 8, *Cfast* Kd n = 10); p values were calculated by Student's t test. (H) Positive correlation of *Cfast* expression and fibrosis genes in mouse hearts 21 days after cardiac injection of *Cfast* depletion lentivirus and ISO-infusion. Pearson's correlation test (r; 95% CI).

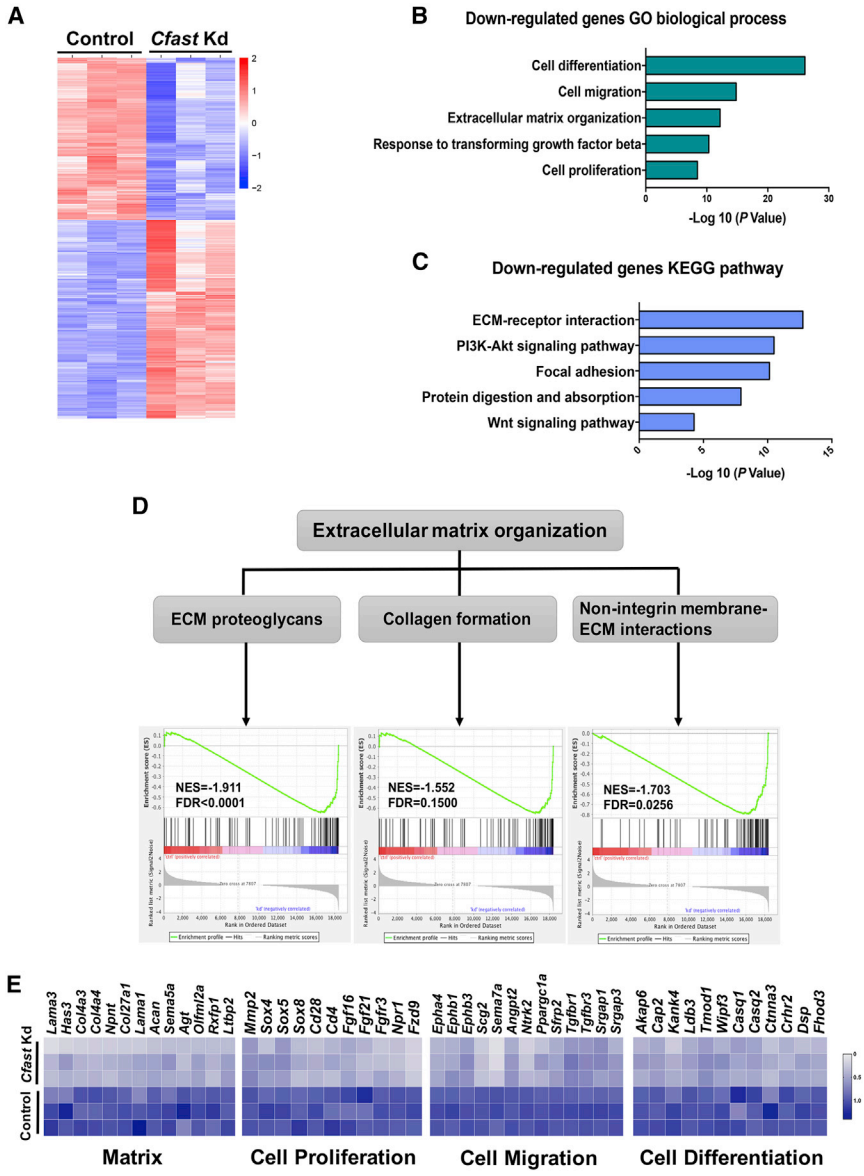

Figure 5. *Cfast* is an important regulator of fibrosis program

(A) Heatmap of differentially expressed gene in *Cfast* knockdown and control cardiac fibroblasts. (fold change, > 2; adjusted $p < 0.05$). (B) Gene Ontology (GO) analysis of downregulated genes. (C) KEGG pathway analysis of downregulated genes. (D) Enrichment plots showing downregulation of genes related to extracellular matrix organization, including ECM proteoglycans, collagen formation, and non-integrin membrane-ECM interactions in *Cfast* knockdown cardiac fibroblasts. (E) Heatmaps of differentially expressed genes related to matrix, cell proliferation, cell migration, and cell differentiation in *Cfast* knockdown cardiac fibroblasts.

To test this hypothesis, we first performed co-immunoprecipitation assays and demonstrated the interaction between COTL1 and TRAP1 (Figure 6D). Interestingly, the interaction between COTL1 and TRAP1 proteins is substantially enhanced when *Cfast* is silenced, indicating that *Cfast* and TRAP1 indeed compete for their association with COLTL1 (Figure 6D). Next, we examined whether COTL1 is sufficient to modulate the activity of the TGF-β signaling and fibrosis program in cardiac fibroblasts. Using an adenovirus-mediated overexpression of COTL1 in cardiac fibroblasts (Figure 6E), we found that COTL1 overexpression inhibited the expression of ECM-related genes, including *Col1a1*, *Col3a1*, and *Fn1* (Figure 6F). Importantly, overexpression of COTL1 in cardiac fibroblasts (Figure 6G), markedly reduced TGF-β induced expression of these ECM related genes (Figure 6H). Furthermore, COTL1 is able to repress the expression of TGF-β activated *Postn* gene, which is a well-known fibroblast activation marker gene (Figure 6H).

An earlier study showed COTL1 inhibits TGF-β signaling in breast cancer via non-canonical signaling involving interleukin-24 (IL-24)/p53 apoptosis effector related to PMP-22 (PERP). We asked whether *Cfast* knockdown affects non-canonical TGF-β signaling by altering the levels of IL-24 and PERP. However, *Cfast* depletion mediated suppression of cardiac fibrosis without affecting the expression levels of IL-24 and PERP in both *in vivo* models of MI and ISO treated hearts, as well as in cardiac fibroblasts *in vitro* (Figures S9A–S9C). Conversely, GSE analysis with RNA-seq data of *Cfast* knockdown in cardiac fibroblasts demonstrated that the TGF-β signaling pathway is downregulated, further supporting the view that *Cfast* regulates the canonical TGF-β signaling pathway in cardiac fibroblasts (Figure 6I). Together, these results indicate that cardiac fibroblast-enriched lncRNA *Cfast* participates in the regulation of ECM gene expression and fibrosis process by modulating the TGF-β signaling pathway (Figure 7).

DISCUSSION

Here, we report the identification and characterization of the cardiac fibroblast-enriched lncRNA *Cfast* and show this lncRNA is an important regulator of cardiac fibrosis. We found that *Cfast* depletion results in a decrease in fibrotic gene expression both *in vitro* and *in vivo*; and most importantly, inhibition of *Cfast* in the heart protects it from pathological fibrotic remodeling and improves cardiac function upon pathological stress. Our results indicate that *Cfast* competitively interacts with COTL1 to prevent the binding of COTL1 from TRAP1, leading to the formation of the TRAP1/SMAD2/SMAD4 complex. As a result, TGF-β signaling is enhanced and fibrotic gene expression

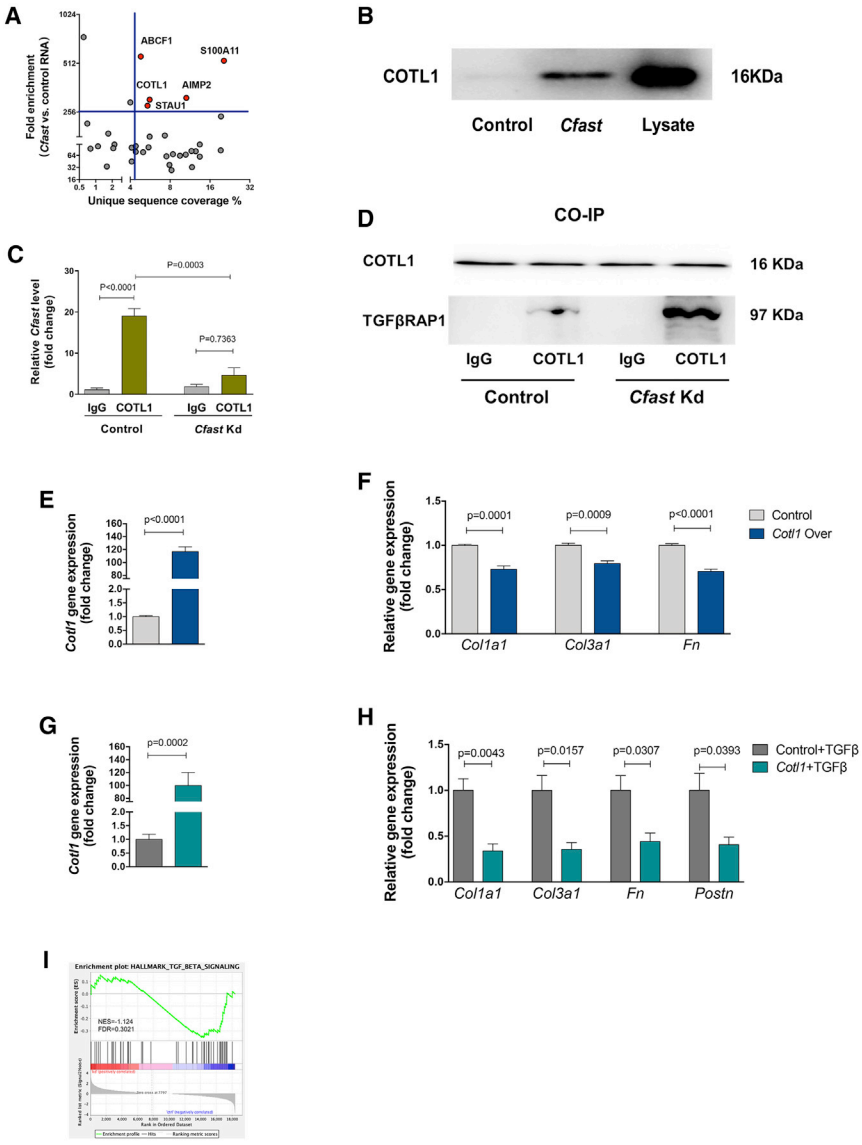

Figure 6. *Cfast* associates with coactosin-like 1 (COTL1) protein to regulate the TGF-β signaling pathway

(A) Summary of distribution of proteins identified from cardiac fibroblasts using *Cfast* RNA pull-down coupled mass spectrometry. (B) Western blot of Cotl1 protein after lncRNA *Cfast* or control pull-down. Whole protein was used as positive control and poly(A) RNA used as negative control. (C) qRT-PCR of *Cfast* level after RNA immunoprecipitation using anti-COTL1 or control antibodies, in control or *Cfast* knockdown cardiac fibroblasts. Graph shows means ± SEM ($n \geq 3$). p values were determined by two-way ANOVA (Sidak's test). (D) Co-immunoprecipitation using anti-COTL1 or control IgG antibodies and western blot using anti-TRAP1 antibody, in control or *Cfast* knockdown cardiac fibroblasts. (E) Cardiac fibroblasts were infected with AD-COTL1 or control and COTL1 expression detected by qRT-PCR. Graph shows means ± SEM ($n \geq 5$). p values were determined by Student's t test. (F) qRT-PCR of the expression of indicated fibrotic genes from cardiac fibroblasts infected with AD-COTL1 or control. Graph shows means ± SEM ($n \geq 5$). p values were determined by Student's t test. (G) Cardiac fibroblasts were infected with AD-COTL1 or control, treated with TGF-β, and COTL1 expression detected by qRT-PCR. Graph shows means ± SEM ($n \geq 5$). p values were determined by Student's t test. (H) qRT-PCR of the expression of indicated fibrotic genes from cardiac fibroblasts infected with AD-COTL1 or control, treated with TGF-β. Graph shows means ± SEM ($n \geq 5$). p values were determined by Student's t test. (I) Gene set enrichment analysis of RNA-seq showed decreased TGF-β signaling in cardiac fibroblasts following *Cfast* knockdown.

increased. Inhibiting *Cfast* expression eventually leads to the repression of this signaling cascade and the reduction of cardiac fibrosis (Figures 7A and 7B). Interestingly, overexpression of COTL1 in CFs markedly reduced the fibrotic response with or without TGF-β treatment, placing COTL1 as a lncRNA binding protein with a protective role in cardiac fibrosis. Therefore, our studies identify *Cfast* as a novel lncRNA and assign its function in cardiac fibroblasts and fibrosis. In addition to its expression in the heart, high *Cfast* expression is also detected in the brain, kidney, liver, and lung. It will be important to determine its function in these organs.

Acute and chronic cardiac injuries and/or stress often result in decrease of cardiac function and cardiomyopathy. Although the damage to the myocardium (cardiomyocytes) is well-established, recent reports indicate that cardiac fibroblasts transdifferentiate into myofibroblasts in response to injuries, which results in the deposition of large amounts of extracellular matrix proteins and the formation of interstitial fibrosis or cardiac scars the development of cardiac fibrosis.[4–6] Several recent studies reported that cardiac fibroblast expressed lncRNAs, including Wisper,[22] Meg3,[23] and Safe,[24] are involved in the regulation of cardiac fibrosis. Mechanistically, it is suggested that Wisper interacts with and modulates the function of TIAR (TIA1-related protein) to control collagen cross-linking and the stabilization of the matrix. On the other hand, Meg3 interacts with transcription factor P53 to control the expression of MMP-2 gene, and, therefore, fibrosis. Our previous studies also linked the expression and function of lncRNAs to atherosclerosis and cardiac fibrosis in mice and humans.[20,21]

We have identified *Cfast* as a novel cardiac fibroblast-enriched lncRNA, and we demonstrated that *Cfast* modulates pathological cardiac fibrosis in two independent models of cardiac remodeling and heart failure. Our investigation shows a distinct molecular mechanism by which lncRNA *Cfast* competitively binds to its partner protein, COTL1, resulting in disassociation of this protein with a

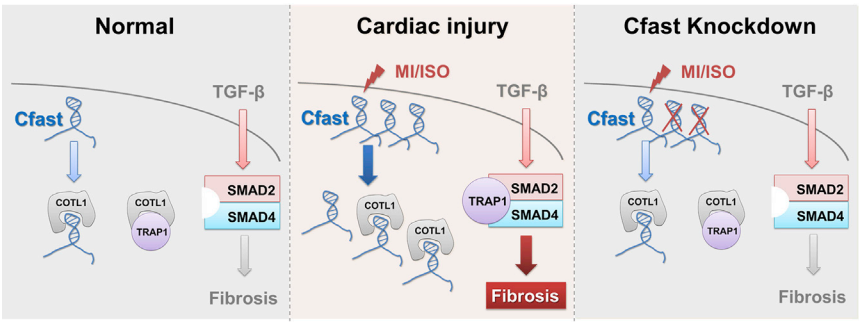

Figure 7. A working model summarizing the function of *Cfast* in TGF-β signaling and fibrotic gene expression

Under normal physiological conditions, *Cfast* transcript associates with COTL1 protein, leaving excessive COTL1 protein to bind to TRAP1. Increased expression of lncRNA *Cfast* under stress conditions results in the association of *Cfast* and COTL1, releasing the COTL1 partner protein TRAP1, which in turn binds to SMAD2/SMAD4 complex to enhance the TGF-β signaling and fibrosis. *Cfast* knockdown allows the association between COTL1 and TRAP1, reducing the formation of the TRAP1/SMAD2/SMAD4 complex, therefore the TGF-β signaling and fibrotic gene expression.

chaperone protein TRAP1, which is important for an essential signaling cascade (i.e., TGF-β) related to fibrotic gene expression and fibrosis (Figure 7). Our study, together with prior reports, reveals that fibroblast-enriched lncRNAs play primary roles in cardiac fibrotic remodeling and cardiac function. These fibroblast specific lncRNAs may have therapeutic potential for fibrosis-related cardiomyopathy.

Although we have offered a molecular explanation by which *Cfast* and COTL1 interact to ultimately modulate the TGF-β signaling pathway in the cardiac fibrotic response, this may not be the exclusive molecular mechanism. Many lncRNAs could exert their roles via sponging microRNAs (miRNAs) and influencing miRNA-targeted mRNAs as competing endogenous RNAs (ceRNAs).[14,16,17,19] However, we have not found promising candidate *Cfast* sponging miRNAs that are directly relevant to cardiac fibrosis, based on bioinformatics analysis. In our study, we focused on *Cfast* binding protein-related molecular mechanisms. Given the complicated regulation of the ceRNA network in pathophysiological processes, future studies will likely expand upon the molecular mechanisms by which *Cfast* contributes to cardiac fibrosis.

In addition to the observation that silencing *Cfast* reduces cardiac fibrosis, we also found that depletion of *Cfast* prevents cardiomyocyte hypertrophy, as evidenced by the blunted fetal gene (*Nppa*, *Nppb*, *Myh7*) reactivation and by the reduction of heart weight verse body weight ratios in both MI- and ISO-induced cardiac injury models, which likely contribute to the improvement of heart function under stress conditions. Intriguingly, the endogenous expression and experimental inhibition of *Cfast* is primarily limited to cardiac fibroblasts, not cardiomyocytes, raising the question of how cardiac fibroblast-enriched *Cfast* affects the function of cardiomyocytes under stress conditions. We speculate that though the functional improvement by *Cfast* depletion is primarily attributed to the prevention of cardiac fibrotic remodeling, there is crosstalk between fibroblasts and cardiomyocytes, which consequently ameliorates hypertrophic remodeling and improves heart function. Our observation does not stand alone—previous studies also document that the fibroblast-enriched lncRNAs, Wisper,[22] and Meg3,[23] exhibit indirect benefits for cardiomyocyte hypertrophy after MI or TAC, respectively, and this may result from paracrine effects.[23]

In addition to COTL1, we also detected four other proteins by mass spectrometry after *Cfast* pulldown; namely, ABCF1, AIMP2, S100A11, and STAU1. There is no evidence that indicates these candidates have direct impact on cardiac fibroblasts and fibrotic remodeling. These proteins are involved in immune responses, cancer development, Parkinson's disease, plasma membrane repair, and cell survival.[28–35] However, whether these candidates are indeed involved in cardiac fibrosis and heart diseases were not examined in the present study. Therefore, we cannot rule out the possibility that their binding with *Cfast* may also impact the behavior of cardiac fibroblasts and cardiac remodeling in response to injury. Clearly, their function associated with *Cfast* warrants further investigation.

In summary, we have identified and characterized lncRNA *Cfast* as a novel regulator of cardiac fibroblasts and fibrotic remodeling in the heart in response to cardiac injuries. *Cfast* exerts its function via binding to COTL1 and, consequently, affects TRAP1/SMAD-mediated fibrotic signaling cascades. Our study indicates that *Cfast* may represent a potential target in antifibrotic RNA therapy in heart diseases.

MATERIALS AND METHODS

Study approvals

The use of animals in this study conformed to the Public Health Service Guide for Care and Use of Laboratory Animals and was approved by the Institutional Animal Care and Use Committee (IACUC) of Boston Children's Hospital and by the IACUC of Zhejiang University. Briefly, mice were maintained on 12 h light:dark cycles and were fed with germ-free diets and fresh sterilized water. For post-operative analgesia, mice were injected with 0.1 mg/kg of Buprenorphine intraperitoneally. Repeated subcutaneous injections of 0.1 mg/kg of Buprenorphine were made every 8 h for 3 days. The human study protocol with using heart tissue from DCM patients and control patients was approved by the Ethics Committee of the Second Affiliated Hospital of Zhejiang University. Patients provided written informed consent.

Microarray-based lncRNA profiling

For microarray analysis, RNAs were prepared from the hearts of mice 3 days after MI surgery (n = 5 hearts) or sham surgery (n = 4 hearts). These RNA samples were subjected to global lncRNA profiling using

the lncRNA Microarray SurePrint G3 Gene Mouse GE 8*60K Kit (Agilent Technologies). Agilent Feature Extraction software (version 11.0.1.1) was used to analyze acquired array images. Quantile-normalization and subsequent data processing were performed with the GeneSpring GX v12.1 software package (Agilent Technologies). Differentially expressed lncRNAs were identified through filtering on FC (≥ 2) and p value ($p < 0.05$).

qRT-PCR

Total RNA was isolated using TRIzol reagent (Life Technologies) from heart tissue or cell samples and was incubated with DNase I (Life Technologies) to remove residual genomic DNA. For detecting gene expression with qRT-PCR, 1.0 μg total RNA samples were reverse transcribed to cDNA using M-MLV reverse transcriptase and random hexamers (Life Technologies) according to the manufacturer's instruction. Primers were designed to span introns. All the qPCR analyses, cDNA prepared without reverse transcriptase was served as a negative control. QPCR Signal was detected by the VII7 Real-time PCR System with SYBR green qPCR Master Mix (Vazyme Biotech). Data were normalized by 18S signal. Primers used for qRT-PCR in this study is listed in Table S3.

RACE

The full-length cDNA sequence of *Cfast* was obtained from mouse hearts RNA by applying RACE according to SMARTer RACE 5′/3′ Kit User Manual (TaKaRa). Nested 5′ and 3′ RACE products were obtained using GXL Taq polymerase with GC Buffer (Takara). The primers used for RACE, nested PCR, and PCR are presented in Table S4. Gel products were extracted with a Gel Extraction kit (Vazyme Biotech), cloned into pMD18-T vectors and analyzed by Sanger sequencing.

RNA fractionation

Nuclear and cytoplasmic RNA fractions of cardiac fibroblasts were isolated using NE-PER Nuclear and Cytoplasmic Extraction Reagents (Thermo Scientific) according to the manufacturer's instructions with addition of RNase inhibitor. The extracted nuclear and cytoplasmic RNA fractions were used to detect *Cfast* content in subcellular localization according to standard qRT-PCR protocol. The expression of glyceraldehyde phosphate dehydrogenase (*Gapdh*) and *β-actin* was used as cytoplasmic controls, whereas the expression of Xist and Neat1 was used as a nuclear control.

Protein coding potential

The protein coding potential of lncRNA candidates was analyzed by using the Coding Potential Calculator (www.cpc.cbi.pku.edu.cn). We used the NCBI ORF Finder (https://www.ncbi.nlm.nih.gov/orffinder/) to identify the potential peptides and then performed mass spectrometry with these total protein lysates of cardiac fibroblasts to detect whether presence of the predicted peptides.

MI and intra-cardiac injection of lentivirus

MI was performed on 8-week-old male c57BL/6 mice (Jackson Laboratory or Shanghai SLAC Laboratory Animal) by ligation of the left anterior descending (LAD) coronary artery.[40,41] For surgery, mice were anesthetized with isoflurane (3% isoflurane for induction, 2% isoflurane for maintenance). After the chest was shaved and cleaned with 75% alcohol, a suture was placed around the front upper incisors and pulled taut so that the neck was slightly extended. For oral intubation, the tongue was retracted and held with forceps, and a 20G catheter was inserted into the trachea. The catheter was then attached to the mouse ventilator via a Y-shaped connector. Ventilation was performed with a tidal volume of 225 μL for a 25 g mouse and a respiratory rate of 130 breaths per minute. 100% oxygen was provided to the inflow of the ventilator. Then the chest was opened through a left parasternal incision, and the heart exposed at the left 3rd–4th intercostal space. Chest retractor was applied to facilitate the view. The pericardium was opened, and the ligation was performed on the LAD coronary artery using 8–0 silk sutures (Ethicon). The lungs were slightly overinflated to assist in removal of air in the pleural cavity. Dissected intercostal space and chest skin were closed using a 6–0 silk suture (Ethicon).

For intra-cardiac injection after MI,[41] mice were randomly subjected to intra-cardiac injection of lentivirus- short hairpin RNAs (shRNA)-*Cfast*, or lentivirus-control ($4–5 \times 10^7$ viral genome particles per mouse heart), respectively after MI. Immediately after the ligation of LAD coronary artery, lentivirus-shRNA-*Cfast*, or lentivirus-control in a total volume of 40 μL were injected into ventricle muscular wall but not ventricular cavity using insulin syringe with needle (31 G). The lentiviruses were evenly injected into five sites around the infarcted area (anterior wall, lateral wall, and apex area). Immediately after injection of lentivirus, anesthesia (isoflurane) was stopped to increase survival. Then the chest was closed, and the animal was changed to a prone position until recovery of spontaneous breathing.

ISO administration and intra-cardiac injection of lentivirus

8-week-old male C3H mice (Beijing Vital River Laboratory Animal Technologies) were administered with ISO hydrochloride (Sigma) to induce cardiac fibrotic remodeling. ISO was dissolved in sterile saline and was injected intraperitoneally (30 mg/kg/day) once daily for 21 consecutive days.[27]

At day 8 of ISO administration, mice were randomly subjected to intra-cardiac injection of lentivirus-shRNA-*Cfast*, or lentivirus-control ($4–5 \times 10^7$ viral genome particles per mouse heart). Mice were orally intubated and maintained with a rodent ventilator for artificial respiration with isoflurane. The chest was opened through a left parasternal incision, and the heart was exposed at the left 3rd–4th intercostal space. Chest retractor was applied to facilitate the view. The pericardium was removed and a total volume of 40 μL of lentivirus-shRNA-*Cfast* or lentivirus-control was intramuscularly injected into anterior left ventricle using insulin syringe with a 31G needle. The lentivirus was evenly injected into five sites around the area of mid-apex of ventricle. The chest was closed, and the animal was changed to a prone position until recovery of spontaneous breathing.

Measurement of cardiac function by echocardiography

Echocardiographic measurements were performed on mice using a Visual Sonics Vevo 2100 Imaging System (Visual Sonics, Toronto, ON, Canada) with a 18–38 MHz transducer (model MS-400).[27,40,41] Mice were anesthetized with isoflurane (2.0% isoflurane for induction and 0.5% for maintenance). Heart rate and left ventricular (LV) dimensions, including diastolic and systolic wall thicknesses, LV end-diastolic, and end-systolic chamber dimensions, were measured from 2-D short-axis under M-mode tracings at the level of the papillary muscle. LV mass and functional parameters such as percentage of fractional shortening (FS%) and LV volume were calculated using the above primary measurements and accompanying software.

Isolation and culture of mouse cardiac fibroblasts

Neonatal mouse cardiac fibroblasts were isolated by enzymatic disassociation according to the manual of neonatal heart dissociation Kit (Miltenyi Biotec, Germany). Briefly, the dissected hearts were transferred into a 10 cm dish with PBS and were trimmed off vessels and connective tissue from ventricles. Then the hearts were dissociated using enzyme mix and gentle MACS C tube for 45 min (gentleMACS Program mr_neoheart_01). After termination of the program, the cells were washed and resuspended in culture medium using MACS SmartStrainer (70 μm). Finally, the collected cells were resuspended and differentially plated for 25 min in DMEM medium containing 10% fetal bovine serum (FBS) and penicillin-streptomycin (100 U/mL). After removing the floating cardiomyocytes, cardiac fibroblasts, readily attached to the bottom, were cultured till passages 2–3 for further assays. After 24 h in serum-free medium, fibroblast cultures were treated with variety as indicated.

Adult mouse cardiac fibroblasts and cardiomyocytes were isolated using a previously reported procedure.[42] Briefly, following perfusion and digestion of the heart with collagenase II (Worthington Biochemical, Lakewood, NJ, USA), dissociated cells were sedimented by gravity. The supernatant, enriched in cardiac fibroblasts, was collected and centrifuged for 5 min at 1,000 rpm. The bottom layer, rich in adult cardiomyocytes, also was collected. The adult cardiac fibroblasts and cardiomyocytes then were treated with Trizol for RNA extraction and qRT-PCR analyses.

Lentivirus construction and infection of lentivirus

Lentiviral expression vectors were used to generate shRNA expression system. The targeting sites of shRNA for lncRNA *Cfast* were designed using the siRNA Wizard (https://www.invivogen.com/sirnawizard/design.php). The sequences for shRNA were listed in Table S5. The lentiviral expression vector, namely pGreenPuro shRNA Cloning and Expression Lentivector, was from System Biosciences. For infection, cells plated at density of 1×10^5 /cm^2, were infected with indicated lentiviruses expressing of shRNA targeting *Cfast* or scramble shRNA as control for 24 h at infection of 50 MOI, and then refreshed with fresh medium. Transfection efficacy was evaluated after 72 h of infection via qRT-PCR or western blot assessments of indicated gene expression levels.

siRNA synthesis and transfection

siRNAs targeting *Cfast* were designed and synthesized by GenePharma (China; sequences listed in Table S5). Targeting siRNAs and scramble siRNA control were transfected into cells at 50 nM of final concentration using Lipofectamine RNAiMAX Reagent (Thermo Scientific).

Western blot analysis

Cultured cells were harvested, homogenized and incubated in Cell Extraction Buffer (Invitrogen) with protease inhibitors cocktail (Sigma) and 1 mM phenylmethylsulfonyl fluoride (PMSF) on ice for 15 min. The lysates were centrifuged at 13,000 × *g* for 10 min at 4°C. After preparation, samples were mixed with Laemmli buffer containing 5% β-mercaptoethanol and were evenly loaded onto SDS-PAGE gels. The separated proteins on gel were then transferred to polyvinylidene fluoride (PVDF) membranes (BioRad). After blocking in 5% BSA, membranes were incubated overnight at 4°C with primary antibody and then washed three times with TBST buffer before incubation for 1 h with HRP-conjugated secondary antibody at room temperature. Protein bands were visualized by using ECL Reagents (Invitrogen) with the Bio-Rad ChemiDoc imaging system. All the antibody information is listed in Table S6.

Histology and immunostaining

Mouse hearts were dissected out, rinsed, and arrested in diastole buffer (4.7 nM KCl and 0.1% 2,3-Butanedione monoxime (BDM) in PBS). Hearts were then fixed in 4% paraformaldehyde (pH 7.4) overnight. After dehydration through a series of ethanol baths, samples were embedded in paraffin wax according to standard laboratory procedures. Sections of 10 μm in thickness were further fixed with prewarmed Bouins' solution at 55 °C for 1 h and stained with Fast Green and Sirius Red.[40,41] The stained sections were used for routine histological examination by light microscopy and polarized light microscopy.

To determine the infarct size, we cut through the embedded paraffin blocks from apex to base. The first 10 sections of every 100 sections were used to stain with Fast Green and Sirius Red. Infarct size was calculated according to the formula: [length of coronal infarct perimeter (epicardial + endocardial) / total LV coronal perimeter (epicardial + endocardial)] × 100.[40,41,43]

Immunofluorescence staining was performed on 4% paraformaldehyde-fixed and paraffin-embedded heart sections.[40,41] After deparaffinization, rehydration, and heat-induced epitope retrieval, sections were incubated with mouse monoclonal anti-myosin heavy chain specific antibody MF20 (5 μg/mL, Developmental Studies Hybridoma Bank) for labeling cardiomyocyte and goat anti-mouse Alexa Fluor 488 secondary antibody (1:400, Invitrogen). The sections were also counterstained with wheat germ agglutinin (WGM; Alexa Fluor 594 conjugate WGA; 1:400, Invitrogen) for labeling fibrotic scar.

Immunofluorescence staining was performed on cultured mouse cardiac fibroblasts for detecting fibroblasts behavior. At the end of

the culture, cells were fixed with 3.7% PFA and then permeabilized with 0.5% Triton/PBS. Then the cells were blocked in 5% goat serum and then incubated with indicated antibodies. To identify myofibroblast transdifferentiation, we used mouse monoclonal anti α-SMA-fluorescein isothiocyanate (FITC) antibody (1:400, Sigma Cat# F3777). To detect fibroblast proliferation, we used rabbit anti phospho-histone H3 (pH3, 1:400, Millipore, cat # 06-570) primary antibody and goat anti-rabbit Alexa Fluor 594 secondary antibody (1:400, Invitrogen). Quantitative data were obtained by measuring co-localization of DAPI (nuclear staining) with α-SMA or pH3 on the fibroblasts. All the antibody information is listed in Table S6.

RNA-seq and genome-wide transcriptome analysis

RNA samples from the cardiac fibroblasts after knockdown of *Cfast* and control were prepared for RNA-seq (three biological replicates for each group). RNA-seq experiments were performed by Novogene (Beijing, China) according to standard procedure.[41] Briefly, total RNA was isolated from cultured cells using TRIzol (Invitrogen). mRNA was then purified from total RNA using poly-T oligo-attached magnetic beads. A total amount of 1 μg RNA per sample was used as input material for the RNA sample preparations. Sequencing libraries were generated using NEBNext UltraTM RNA Library Prep Kit for Illumina (NEB, USA) following manufacturer's recommendations, and index codes were added to attribute sequences to each sample. The clustering of the index-coded samples was performed on a cBot Cluster Generation System using TruSeq PE Cluster Kit v3-cBot-HS (Illumia) according to the manufacturer's instructions. After cluster generation, the library preparations were sequenced on an Illumina Hiseq platform and 150 bp paired-end reads were generated. For the data analysis, raw data (raw reads) in fastq format were first processed through in-house Perl scripts. Clean data (clean reads) were obtained by removing reads containing adapters, reads containing ploy-N and low-quality reads from raw data. Reference genome and gene model annotation files were downloaded from genome website directly. Index of the reference genome was built using STAR and paired-end clean reads were aligned to the reference genome using STAR (v2.5.1b). STAR uses the method of Maximal Mappable Prefix (MMP). HTSeq v0.6.0 was used to count the read numbers mapped to each gene. Analysis of differential expression was performed using the edgeR R package (3.12.1). The p values were adjusted using the Benjamini and Hochberg method. GO and KEGG pathway analyses were implemented using the clusterProfiler R package. The hierarchical clustering heatmap was generated with the ggplot library.

Cfast RNA pull-down

Biotinylated *Cfast* sense and control RNA (poly[A]) were *in vitro* transcribed using the T7 RNA polymerase (Invitrogen MEGAscript T7 Transcription Kit) and Biotin RNA Labeling Mix (Thermo Scientific, Pierce RNA 3′ End Desthiobiotinylation Kit) and then purified according to the manufacturers' instructions. Biotinylated RNA was incubated with magnetic bead (Thermo Scientific, Pierce Magnetic RNA-Protein Pull-Down Kit), and then incubated with cardiac fibroblast lysate for 4 h. The samples were separated via SDS-PAGE and identified using mass spectrometry and retrieved in mouse proteomic library.

RIP and protein co-immunoprecipitation

RIP experiments were performed with DynabeadsTM magnetic beads (Thermo Scientific, Dynabeads Protein G) according to the manufacturer's instructions. Briefly, we constructed a COTL1 and FLAG fusion protein in adenovirus and overexpressed the COTL1-FLAG in 3T3 cell line. Thereafter, $\sim 2 \times 10^8$ 3T3 cells were lysed thoroughly on ice in NP40 Cell Lysis Buffer (Thermo Scientific) supplemented with protease inhibitor cocktail and RNase inhibitor. 10 μg of FLAG antibodies (Table S6) or isotype control immunoglobulin G (IgG) were respectively incubated with magnetic beads at room temperature for 30 min for each immunoprecipitation. Lysate proteins were incubated with indicated antibody-beads complex overnight at 4°C with rotating. Co-immunoprecipitated RNAs were extracted, reverse-transcribed to cDNA, and subjected to qPCR examination. Co-immunoprecipitated proteins were analysis by western blot.

Statistical analysis

Unless otherwise stated, results were presented as mean value ± standard error of the mean (SEM). GraphPad Software (version 7) was used for statistical analysis. Statistical significance between two columns was assessed by two-tailed unpaired Student's t test; for more than two columns, one-way ANOVA (Dunnett's multiple comparisons test) analysis was used. Two-way ANOVA (Sidak's test) was used to evaluate statistical significance between two or more groups. Correlation analysis was performed with Pearson (r or r2 values; 95% confidence interval [CI]) or Spearman (r; 95% CI) test. A value of $p < 0.05$ was considered statistically significant.

DATA AVAILABILITY

RNA-seq data (GEO: GSE161389) and microarray-based transcriptome profiling data (GEO: GSE161427) are available in the Gene Expression Omnibus.

SUPPLEMENTAL INFORMATION

Supplemental Information can be found online at https://doi.org/10.1016/j.omtn.2020.11.013.

ACKNOWLEDGMENTS

The authors thank the Core Facilities of Institute of Translational Medicine, Zhejiang University School of Medicine, and the Laboratory Animal Center of Zhejiang University. This work is supported by National Key R&D Program of China (2017YFA0103700); Zhejiang Provincial NSF project (LZ20H020001 to J.C.); National Natural Science Foundation of China (numbers 81470382, 81670257, and 81970227 to J.C., 81873463 to Z.-P.H., and 82000244 to F.G.,); China Postdoctoral Science Foundation (2020M671751 to F.G.); and Guangdong Science and Technology Department (2018A050506026 to Z.-P.H.). Work in the Wang lab is supported by NIH grant HL125925.

AUTHOR CONTRIBUTIONS

J.C. and D.-Z.W. conceived of and designed the study and wrote and revised the manuscript. F.Z. and X.F. designed the experiments, analyzed the data, and drafted the manuscript. M.K., N.L., Y.W., F.G., T.L., X.D., J.P., and X.H. analyzed and interpreted the data. W.Z., H.Y., D.B.C., X.H., Z.-P.H., and J.W. refined the data analysis and reviewed the manuscript.

DECLARATION OF INTEREST

The authors declare no competing interests.

REFERENCES

1. Roth, G.A., Johnson, C., Abajobir, A., Abd-Allah, F., Abera, S.F., Abyu, G., Ahmed, M., Aksut, B., Alam, T., Alam, K., et al. (2017). Global, Regional, and National Burden of Cardiovascular Diseases for 10 Causes, 1990 to 2015. J. Am. Coll. Cardiol. *70*, 1–25.
2. Frangogiannis, N.G. (2019). Cardiac fibrosis: Cell biological mechanisms, molecular pathways and therapeutic opportunities. Mol. Aspects Med. *65*, 70–99.
3. Berk, B.C., Fujiwara, K., and Lehoux, S. (2007). ECM remodeling in hypertensive heart disease. J. Clin. Invest. *117*, 568–575.
4. Prabhu, S.D., and Frangogiannis, N.G. (2016). The Biological Basis for Cardiac Repair After Myocardial Infarction: From Inflammation to Fibrosis. Circ. Res. *119*, 91–112.
5. Gourdie, R.G., Dimmeler, S., and Kohl, P. (2016). Novel therapeutic strategies targeting fibroblasts and fibrosis in heart disease. Nat. Rev. Drug Discov. *15*, 620–638.
6. Tallquist, M.D., and Molkentin, J.D. (2017). Redefining the identity of cardiac fibroblasts. Nat. Rev. Cardiol. *14*, 484–491.
7. Ponting, C.P., Oliver, P.L., and Reik, W. (2009). Evolution and functions of long noncoding RNAs. Cell *136*, 629–641.
8. Batista, P.J., and Chang, H.Y. (2013). Long noncoding RNAs: cellular address codes in development and disease. Cell *152*, 1298–1307.
9. Uchida, S., and Dimmeler, S. (2015). Long noncoding RNAs in cardiovascular diseases. Circ. Res. *116*, 737–750.
10. Viereck, J., and Thum, T. (2017). Long Noncoding RNAs in Pathological Cardiac Remodeling. Circ. Res. *120*, 262–264.
11. Cremer, S., Michalik, K.M., Fischer, A., Pfisterer, L., Jaé, N., Winter, C., Boon, R.A., Muhly-Reinholz, M., John, D., Uchida, S., et al. (2019). Hematopoietic Deficiency of the Long Noncoding RNA MALAT1 Promotes Atherosclerosis and Plaque Inflammation. Circulation *139*, 1320–1334.
12. Han, P., Li, W., Lin, C.H., Yang, J., Shang, C., Nuernberg, S.T., Jin, K.K., Xu, W., Lin, C.Y., Lin, C.J., et al. (2014). A long noncoding RNA protects the heart from pathological hypertrophy. Nature *514*, 102–106.
13. Viereck, J., Kumarswamy, R., Foinquinos, A., Xiao, K., Avramopoulos, P., Kunz, M., Dittrich, M., Maetzig, T., Zimmer, K., Remke, J., et al. (2016). Long noncoding RNA Chast promotes cardiac remodeling. Sci. Transl. Med. *8*, 326ra22.
14. Wang, K., Liu, F., Zhou, L.Y., Long, B., Yuan, S.M., Wang, Y., Liu, C.Y., Sun, T., Zhang, X.J., and Li, P.F. (2014). The long noncoding RNA CHRF regulates cardiac hypertrophy by targeting miR-489. Circ. Res. *114*, 1377–1388.
15. Wang, Z., Zhang, X.J., Ji, Y.X., Zhang, P., Deng, K.Q., Gong, J., Ren, S., Wang, X., Chen, I., Wang, H., et al. (2016). The long noncoding RNA Chaer defines an epigenetic checkpoint in cardiac hypertrophy. Nat. Med. *22*, 1131–1139.
16. Cai, B., Ma, W., Ding, F., Zhang, L., Huang, Q., Wang, X., Hua, B., Xu, J., Li, J., Bi, C., et al. (2018). The Long Noncoding RNA CAREL Controls Cardiac Regeneration. J. Am. Coll. Cardiol. *72*, 534–550.
17. Chen, G., Li, H., Li, X., Li, B., Zhong, L., Huang, S., Zheng, H., Li, M., Jin, G., Liao, W., et al. (2018). Loss of long non-coding RNA CRRL promotes cardiomyocyte regeneration and improves cardiac repair by functioning as a competing endogenous RNA. J. Mol. Cell. Cardiol. *122*, 152–164.
18. Ponnusamy, M., Liu, F., Zhang, Y.H., Li, R.B., Zhai, M., Liu, F., Zhou, L.Y., Liu, C.Y., Yan, K.W., Dong, Y.H., et al. (2019). Long Noncoding RNA CPR (Cardiomyocyte Proliferation Regulator) Regulates Cardiomyocyte Proliferation and Cardiac Repair. Circulation *139*, 2668–2684.
19. Wang, J., Chen, X., Shen, D., Ge, D., Chen, J., Pei, J., Li, Y., Yue, Z., Feng, J., Chu, M., and Nie, Y. (2019). A long noncoding RNA NR_045363 controls cardiomyocyte proliferation and cardiac repair. J. Mol. Cell. Cardiol. *127*, 105–114.
20. Wu, G., Cai, J., Han, Y., Chen, J., Huang, Z.P., Chen, C., Cai, Y., Huang, H., Yang, Y., Liu, Y., et al. (2014). LincRNA-p21 regulates neointima formation, vascular smooth muscle cell proliferation, apoptosis, and atherosclerosis by enhancing p53 activity. Circulation *130*, 1452–1465.
21. Huang, Z.P., Ding, Y., Chen, J., Wu, G., Kataoka, M., Hu, Y., Yang, J.H., Liu, J., Drakos, S.G., Selzman, C.H., et al. (2016). Long non-coding RNAs link extracellular matrix gene expression to ischemic cardiomyopathy. Cardiovasc. Res. *112*, 543–554.
22. Micheletti, R., Plaisance, I., Abraham, B.J., Sarre, A., Ting, C.C., Alexanian, M., Maric, D., Maison, D., Nemir, M., Young, R.A., et al. (2017). The long noncoding RNA *Wisper* controls cardiac fibrosis and remodeling. Sci. Transl. Med. *9*, eaai9118.
23. Piccoli, M.T., Gupta, S.K., Viereck, J., Foinquinos, A., Samolovac, S., Kramer, F.L., Garg, A., Remke, J., Zimmer, K., Batkai, S., and Thum, T. (2017). Inhibition of the Cardiac Fibroblast-Enriched lncRNA *Meg3* Prevents Cardiac Fibrosis and Diastolic Dysfunction. Circ. Res. *121*, 575–583.
24. Hao, K., Lei, W., Wu, H., Wu, J., Yang, Z., Yan, S., Lu, X.A., Li, J., Xia, X., Han, X., et al. (2019). LncRNA-*Safe* contributes to cardiac fibrosis through *Safe-Sfrp2*-HuR complex in mouse myocardial infarction. Theranostics *9*, 7282–7297.
25. Fu, X., Khalil, H., Kanisicak, O., Boyer, J.G., Vagnozzi, R.J., Maliken, B.D., Sargent, M.A., Prasad, V., Valiente-Alandi, I., Blaxall, B.C., and Molkentin, J.D. (2018). Specialized fibroblast differentiated states underlie scar formation in the infarcted mouse heart. J. Clin. Invest. *128*, 2127–2143.
26. Kong, L., Zhang, Y., Ye, Z.Q., Liu, X.Q., Zhao, S.Q., Wei, L., and Gao, G. (2007). CPC: assess the protein-coding potential of transcripts using sequence features and support vector machine. Nucleic Acids Res. *35*, W345–W349.
27. Huang, Z.P., Chen, J., Seok, H.Y., Zhang, Z., Kataoka, M., Hu, X., and Wang, D.Z. (2013). MicroRNA-22 regulates cardiac hypertrophy and remodeling in response to stress. Circ. Res. *112*, 1234–1243.
28. Arora, H., Wilcox, S.M., Johnson, L.A., Munro, L., Eyford, B.A., Pfeifer, C.G., Welch, I., and Jefferies, W.A. (2019). The ATP-Binding Cassette Gene ABCF1 Functions as an E2 Ubiquitin-Conjugating Enzyme Controlling Macrophage Polarization to Dampen Lethal Septic Shock. Immunity *50*, 418–431.
29. Wilcox, S.M., Arora, H., Munro, L., Xin, J., Fenninger, F., Johnson, L.A., Pfeifer, C.G., Choi, K.B., Hou, J., Hoodless, P.A., and Jefferies, W.A. (2017). The role of the innate immune response regulatory gene ABCF1 in mammalian embryogenesis and development. PLoS ONE *12*, e0175918.
30. Lim, S., Cho, H.Y., Kim, D.G., Roh, Y., Son, S.Y., Mushtaq, A.U., Kim, M., Bhattarai, D., Sivaraman, A., Lee, Y., et al. (2020). Targeting the interaction of AIMP2-DX2 with HSP70 suppresses cancer development. Nat. Chem. Biol. *16*, 31–41.
31. Lee, Y., Karuppagounder, S.S., Shin, J.H., Lee, Y.I., Ko, H.S., Swing, D., Jiang, H., Kang, S.U., Lee, B.D., Kang, H.C., et al. (2013). Parthanatos mediates AIMP2-activated age-dependent dopaminergic neuronal loss. Nat. Neurosci. *16*, 1392–1400.
32. Yun, S.P., Kim, H., Ham, S., Kwon, S.H., Lee, G.H., Shin, J.H., Lee, S.H., Ko, H.S., and Lee, Y. (2017). VPS35 regulates parkin substrate AIMP2 toxicity by facilitating lysosomal clearance of AIMP2. Cell Death Dis. *8*, e2741.
33. Jaiswal, J.K., Lauritzen, S.P., Scheffer, L., Sakaguchi, M., Bunkenborg, J., Simon, S.M., Kallunki, T., Jäättelä, M., and Nylandsted, J. (2014). S100A11 is required for efficient plasma membrane repair and survival of invasive cancer cells. Nat. Commun. *5*, 3795.
34. Gong, C., and Maquat, L.E. (2011). lncRNAs transactivate STAU1-mediated mRNA decay by duplexing with 3′ UTRs via Alu elements. Nature *470*, 284–288.
35. Jeong, K., Ryu, I., Park, J., Hwang, H.J., Ha, H., Park, Y., Oh, S.T., and Kim, Y.K. (2019). Staufen1 and UPF1 exert opposite actions on the replacement of the nuclear cap-binding complex by eIF4E at the 5′ end of mRNAs. Nucleic Acids Res. *47*, 9313–9328.
36. Xia, L., Xiao, X., Liu, W.L., Song, Y., Liu, T.J.J., Li, Y.J., Zacksenhaus, E., Hao, X.J., and Ben-David, Y. (2018). Coactosin-like protein CLP/Cotl1 suppresses breast cancer growth through activation of IL-24/PERP and inhibition of non-canonical TGFβ signaling. Oncogene *37*, 323–331.

37. Li, G., Yin, Y., Chen, J., Fan, Y., Ma, J., Huang, Y., Chen, C., Dai, P., Chen, S., and Zhao, S. (2018). Coactosin-like protein 1 inhibits neuronal migration during mouse corticogenesis. J. Vet. Sci. *19*, 21–26.

38. Provost, P., Samuelsson, B., and Rådmark, O. (1999). Interaction of 5-lipoxygenase with cellular proteins. Proc. Natl. Acad. Sci. USA *96*, 1881–1885.

39. Wurthner, J.U., Frank, D.B., Felici, A., Green, H.M., Cao, Z., Schneider, M.D., McNally, J.G., Lechleider, R.J., and Roberts, A.B. (2001). Transforming growth factor-beta receptor-associated protein 1 is a Smad4 chaperone. J. Biol. Chem. *276*, 19495–19502.

40. Chen, J., Huang, Z.P., Seok, H.Y., Ding, J., Kataoka, M., Zhang, Z., Hu, X., Wang, G., Lin, Z., Wang, S., et al. (2013). mir-17-92 cluster is required for and sufficient to induce cardiomyocyte proliferation in postnatal and adult hearts. Circ. Res. *112*, 1557–1566.

41. Gao, F., Kataoka, M., Liu, N., Liang, T., Huang, Z.P., Gu, F., Ding, J., Liu, J., Zhang, F., Ma, Q., et al. (2019). Therapeutic role of miR-19a/19b in cardiac regeneration and protection from myocardial infarction. Nat. Commun. *10*, 1802.

42. Chen, J., Shearer, G.C., Chen, Q., Healy, C.L., Beyer, A.J., Nareddy, V.B., Gerdes, A.M., Harris, W.S., O'Connell, T.D., and Wang, D. (2011). Omega-3 fatty acids prevent pressure overload-induced cardiac fibrosis through activation of cyclic GMP/protein kinase G signaling in cardiac fibroblasts. Circulation *123*, 584–593.

43. Pfeffer, J.M., Pfeffer, M.A., Fletcher, P.J., and Braunwald, E. (1991). Progressive ventricular remodeling in rat with myocardial infarction. Am. J. Physiol. *260*, H1406–H1414.

OMTN, Volume *23*

Supplemental Information

Long noncoding RNA *Cfast* regulates cardiac fibrosis

Feng Zhang, Xuyang Fu, Masaharu Kataoka, Ning Liu, Yingchao Wang, Feng Gao, Tian Liang, Xiaoxuan Dong, Jianqiu Pei, Xiaoyun Hu, Wei Zhu, Hong Yu, Douglas B. Cowan, Xinyang Hu, Zhan-Peng Huang, Jian'an Wang, Da-Zhi Wang, and Jinghai Chen

Supplemental Figure 1.

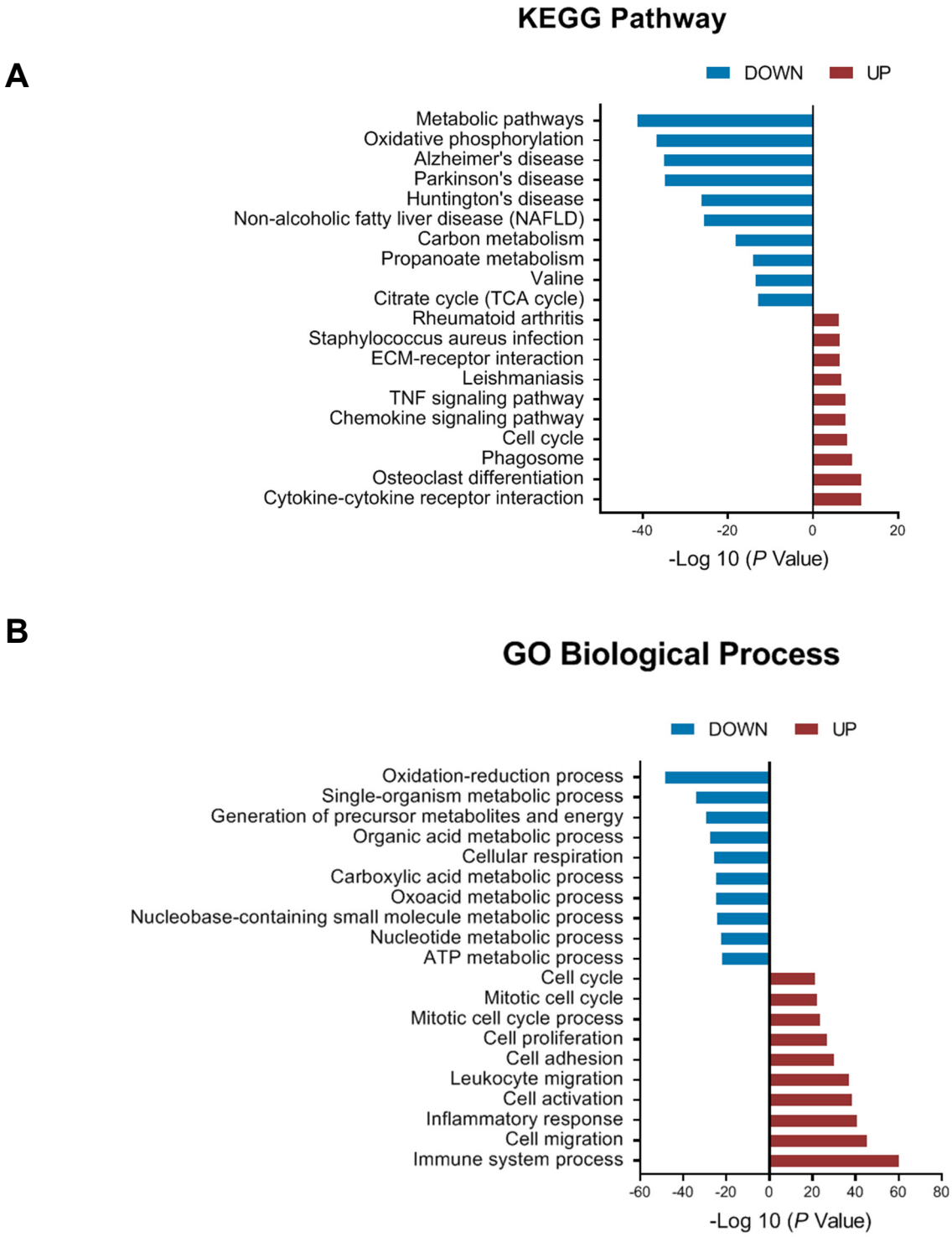

Supplemental Figure 1. Analysis of microarray data after 3days myocardial infarction (MI). (A and B) KEGG pathway (A) and GO terms linked to biological process(B) for the up-regulated and down-regulated genes after myocardial infarction.

Supplemental Figure 2.

A

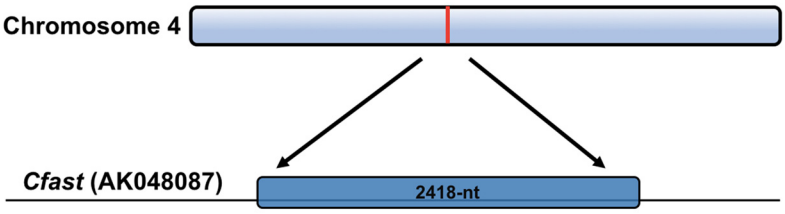

B

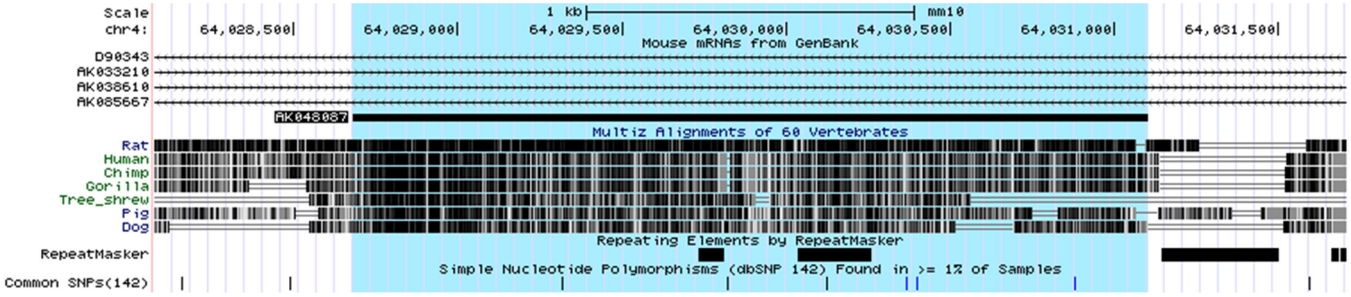

C

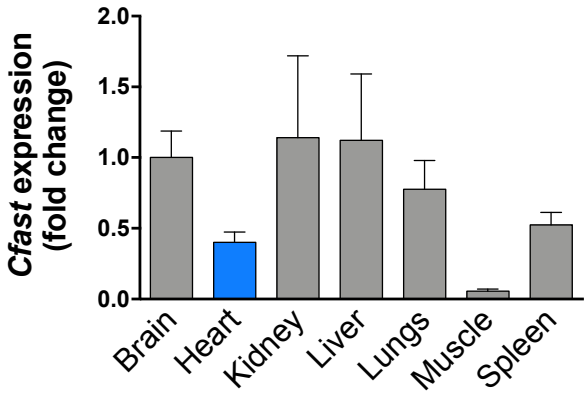

Supplemental Figure 2. Structure of lncRNA *Cfast* and its expression in different tissues.

(A) The lncRNA Cfast is located on chromosome 4 and appears to a single exon transcript.

(B) Conservation of *Cfast* in the mouse, Rat, Human, Chimp, Gorilla, Pig, Dog. The horizontal lines indicate the mouse *Cfast*. The black boxes show the conserved sequences of *Cfast* in Rat, Human, Chimp, Gorilla, Pig, Dog.

(C) Expression of Cfast in different tissues from adult mice. Data represent mean ± SEM (n = 3).

Supplemental Figure 3.

A

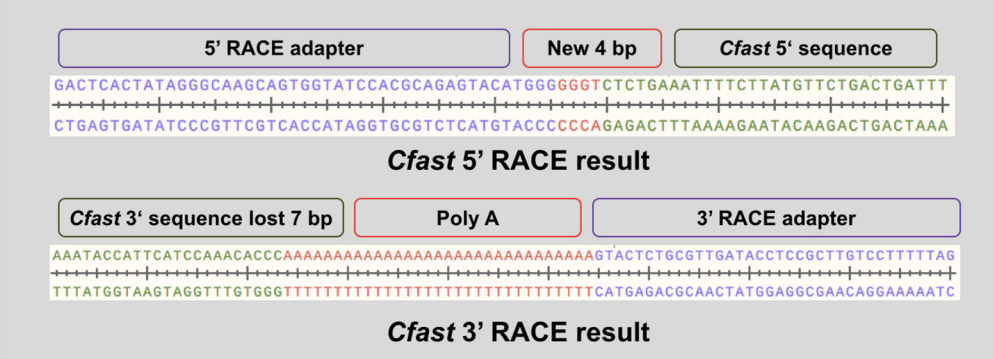

B

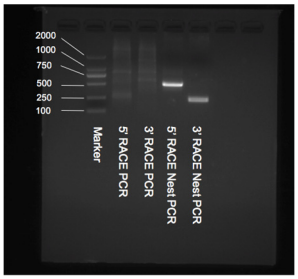

C

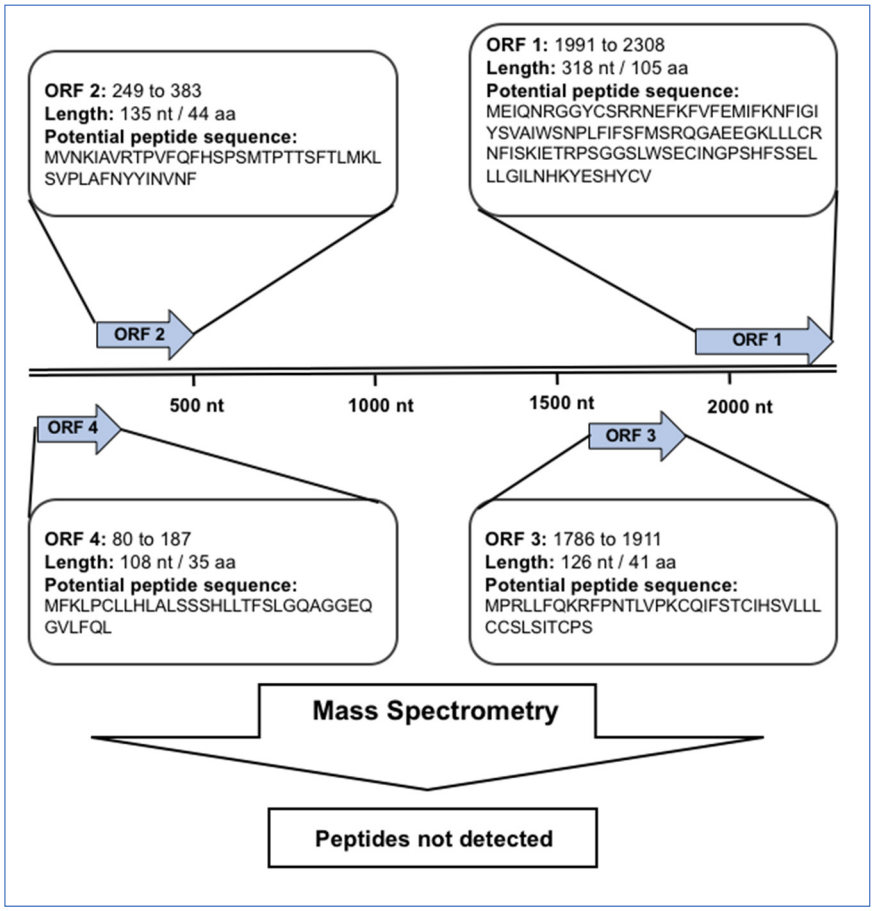

Supplemental Figure 3. *Cfast* is a long non-coding RNA.

(A) Graphical representation of 3′ and 5′ rapid amplification of cDNA (complementary DNA) ends (RACE) results of Cfast.

(B) PCR product Gel image of 3′ and 5′ RACE of Cfast

(C) Presentation of the open reading frames (ORFs) potentially encoded by the Cfast sequence.

Supplemental Figure 4.

A

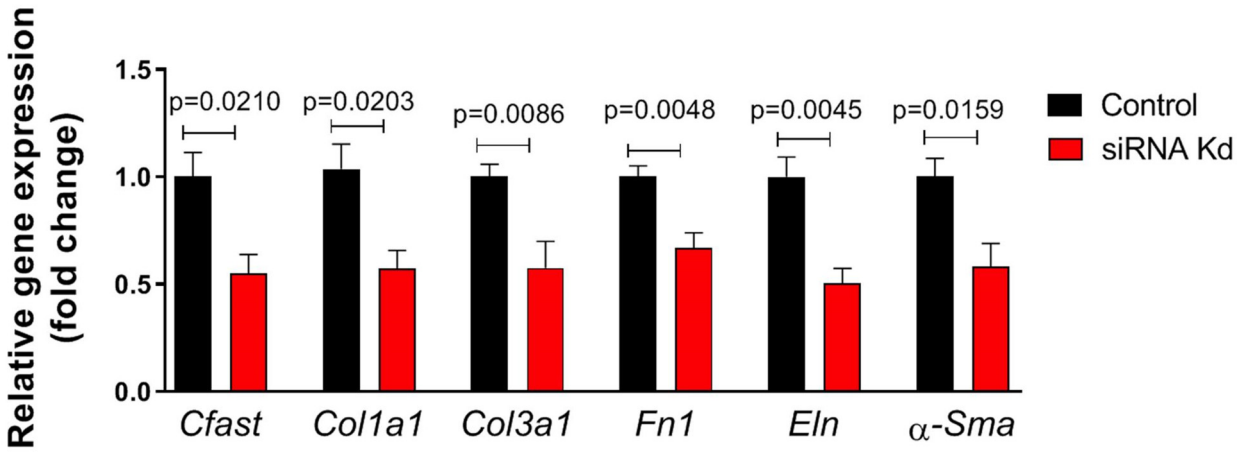

Supplemental Figure 4 Knock-down of *Cfast* by siRNA inhibits expression of cardiac fibrotic genes.
(A) qRT-PCR of Cfast and fibrosis genes in control and Cfast siRNA treated cardiac fibroblasts. n≥4, P values were determined by Student's t test..

Supplemental Figure 5.

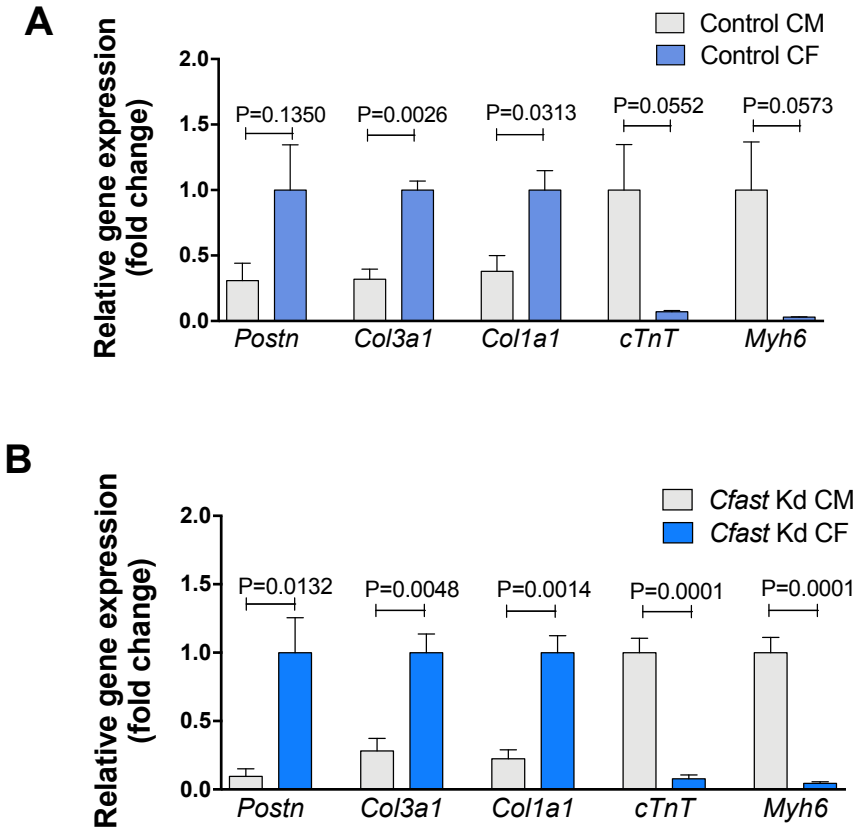

Supplemental Figure 5 Expression of cardiomyocyte and cardiac fibroblast gene expression in mouse hearts after Cfast knockdown.
8 weeks old adult mice were subjected to myocardial infarction surgery. Immediately after MI surgery, control (Control) or *Cfast* knocking down lentivirus (*Cfast* Kd) was injected into myocardium adjacent to the infarcted area. Seven days later, cardiomyocytes (CM)and cardiac fibroblasts (CF) were isolated from the hearts of Control (A) or Cfast kd (B) mice. Expression of cardiomyocyte (cTNT, Myh6) or cardiac fibroblast (Postn, Col3a1, Col1a1) marker genes was determined by qRT-PCR. Data was represented as (CM/CF) ratio over mean fold change ± SEM (n ≥3). P value was determined by Student's t test.

Supplemental Figure 6.

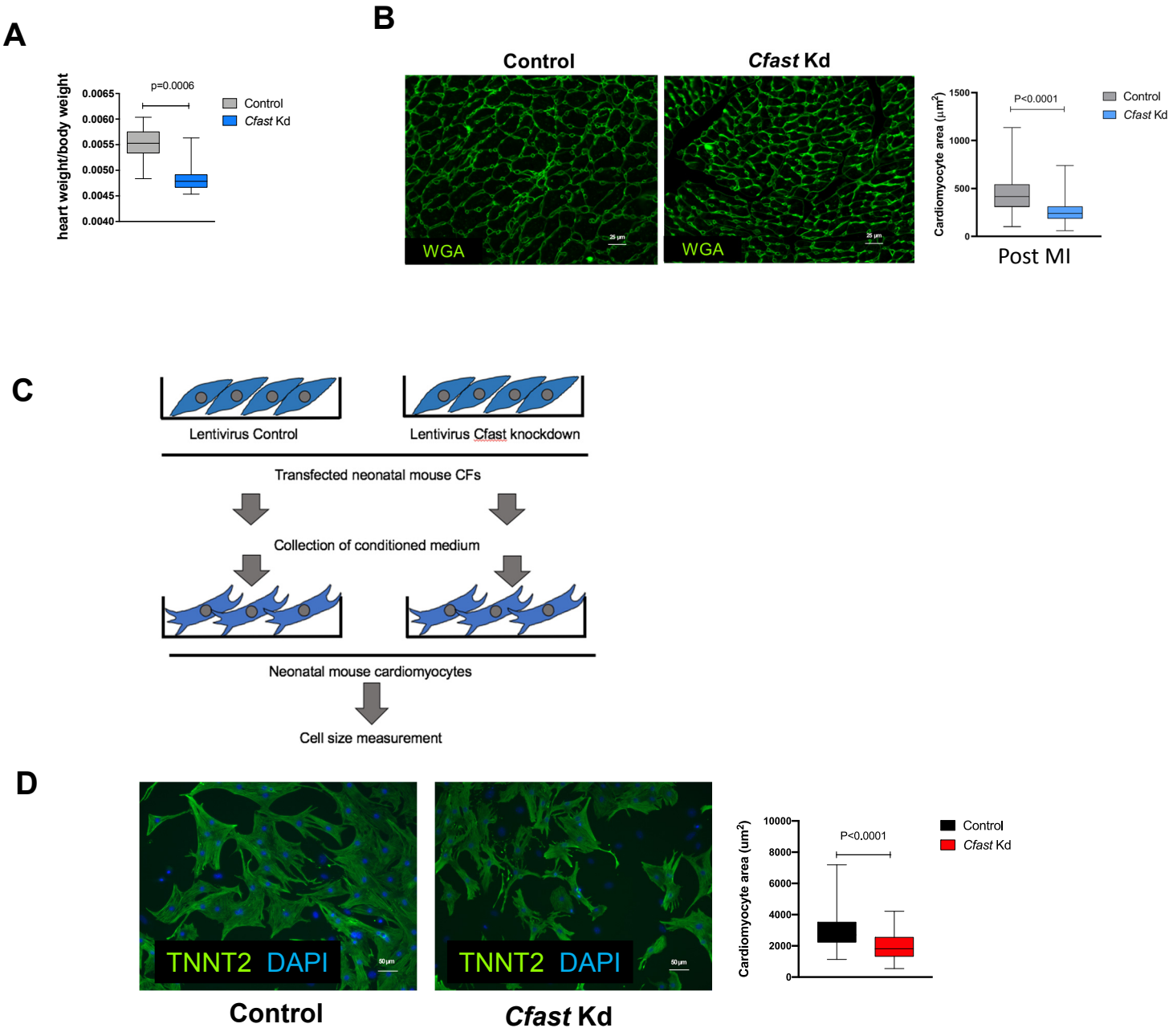

Supplemental Figure 6 Cfast knocking down reduces cardiomyocyte hypertrophy post MI.
(A) Heart weight to body weight ratio of mouse hearts 28 days after cardiac-injection of Cfast depletion lentivirus and MI (Control n= 8, Cfast Kd n=10). P value was determined by Student's t test.
(B) Determination of cardiomyocyte cross-sectional area in histological sections stained with wheat germ agglutinin (WGA, green) from control and Cfast Kd groups post-MI (scale bar=25 μm, n=6/6). P value was determined by Student's t test.
(C) Neonatal cardiac fibroblasts (CFs) have been transfected with lentivirus control or lentivirus Cfast knockdown. The conditioned medium was collected 48 hours after transfection and added to cultured neonatal mouse cardiomyocytes (NMCMs). Cell sizes were measured 48 hours after addition of CF-conditioned medium.
(D) NMCMs cultured in CFs conditioned medium for 48 hours were then stained with TNNT2 (Green) for cardiomyocytes and DAPI (blue) for nuclear. Cell size measurement in NMCMs (n=4 independent replicates, 127-127 cells each, scale bar=50 μm). P value was determined by Student's t test.

Supplemental Figure 7.

A

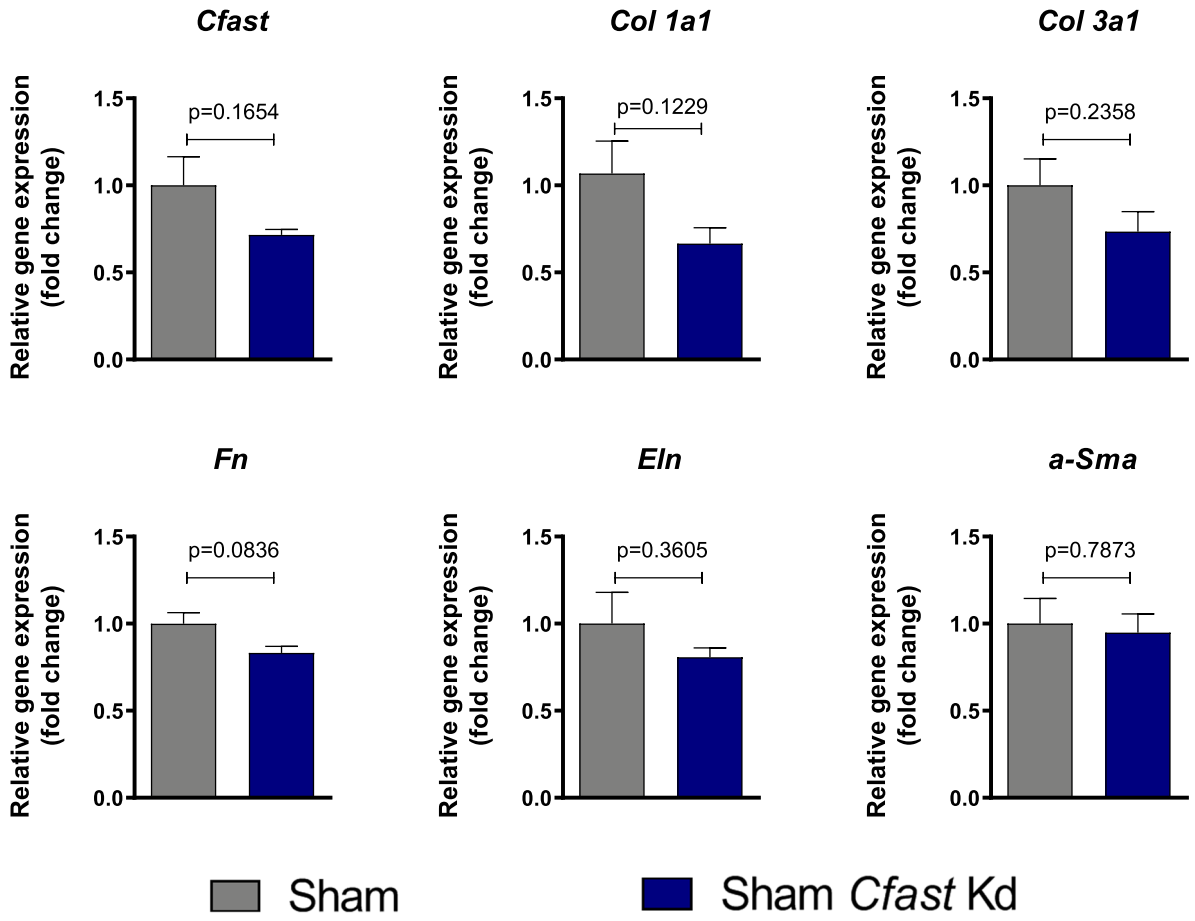

Supplemental Figure 7 Knock-down of Cfast does not affect fibrotic gene in Sham.

(A) qRT-PCR of Cfast and fibrosis genes in Cfast depletion and control treated with sham. n=3, P values were determined by Student's t test..

Supplemental Figure 8.

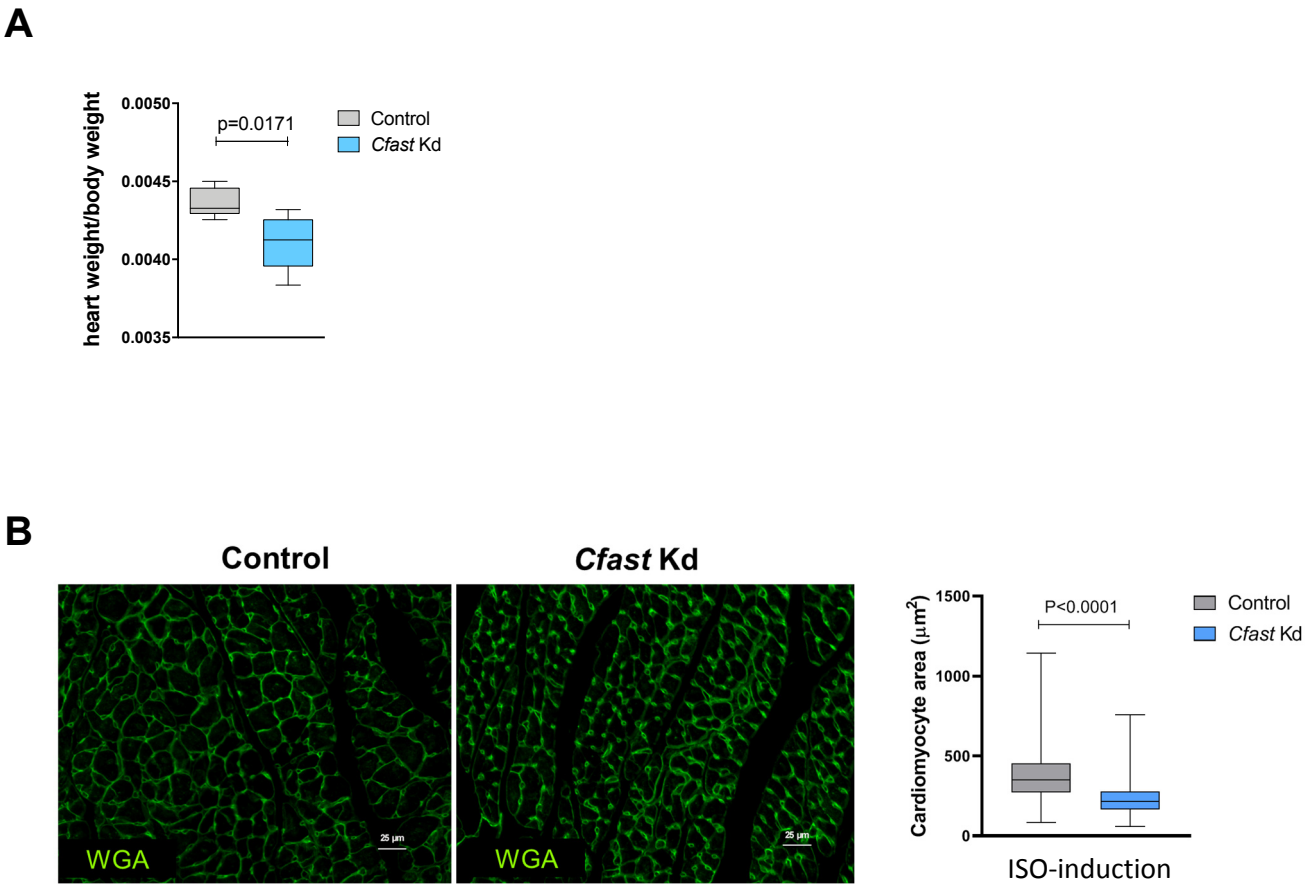

Supplemental Figure 8. Cfast knocking down reduces cardiac hypertrophy post ISO treatment.

(A) Heart weight to body weight ratio of mouse hearts 21 days after cardiac injection of Cfast depletion lentivirus and ISO-infusion. Bars represent means normalized to Control ± SEM(n=6). P value was determined by Student's t test.

(B) Determination of cardiomyocyte cross-sectional area in histological sections stained with wheat germ agglutinin (WGA, green) from control and Cfast Kd groups post-ISO treatment (scale bar=25 μm, n=6/6). P value was determined by Student's t test.

Supplemental Figure 9.

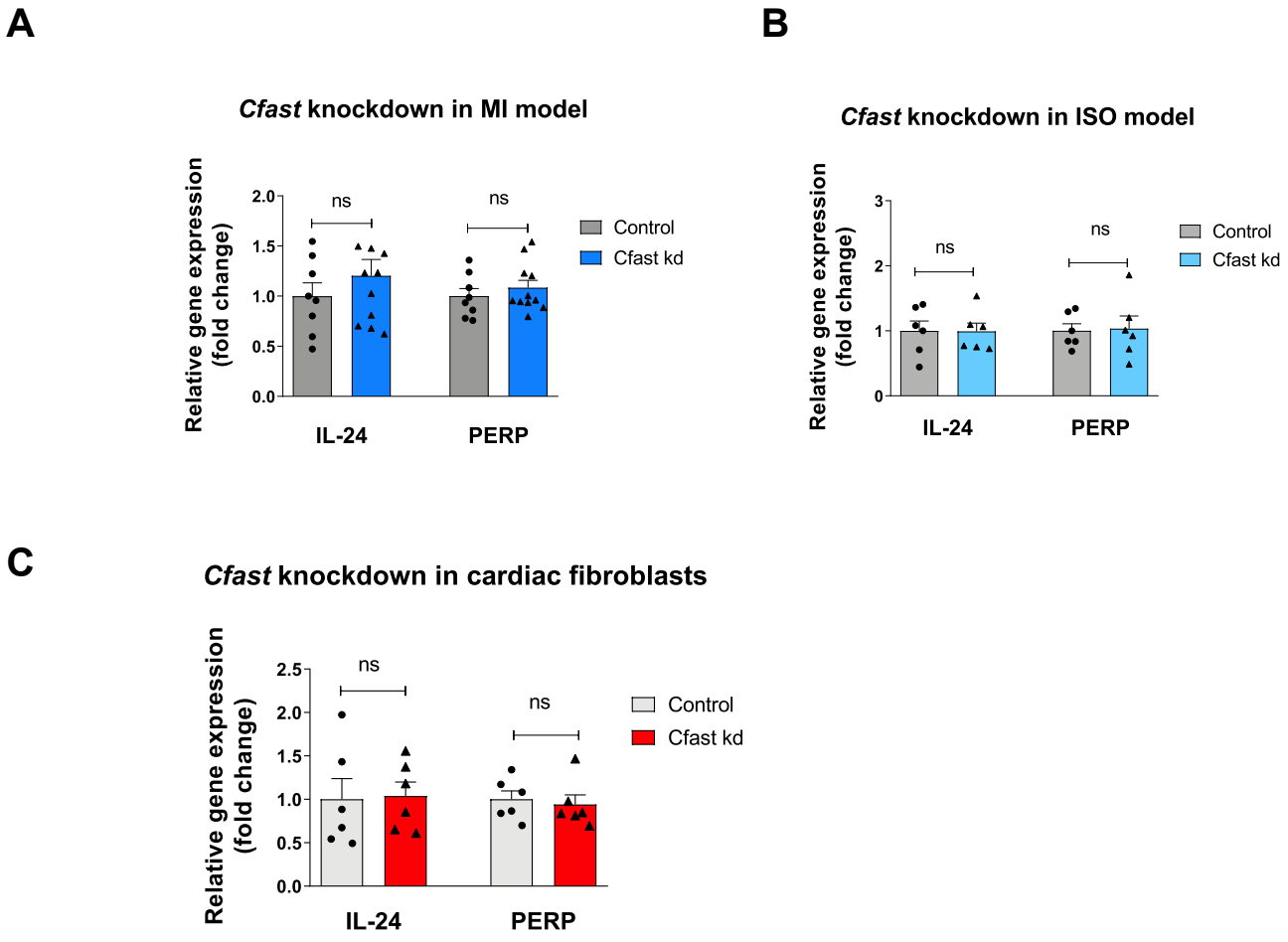

Supplemental Figure 9. Impact of *Cfast* knocking down in non-canonical TGF-beta signaling.
(A-C) Level of IL-24 and PERP were determined by qRT-PCR on the samples of Cfast knocking down and control groups in both in vivo model of (A) myocardial infarction (MI) and (B) isoproterenol (ISO) treated hearts, as well as (C) in vitro model of isolated cardiac fibroblasts. n=6, P values were determined by Student's t test..

List of Supplemental Tables

Supplemental Table 1. Echocardiography examination of cardiac function after *Cfast*-depletion and 4-week of myocardial infraction or Sham

Echocardiography examination of cardiac function after *Cfast*-depletion and 4-week of myocardial infraction (MI)													
Group	**Ear tag**	**IVS;d**	**IVS;s**	**LVID;d**	**LVID;s**	**LVPW;d**	**LVPW;s**	**EF**	**FS**	**LV Mass**	**LV Mass (Corrected)**	**LV Vol;d**	**LV Vol;s**
Control + MI	5161	1.04386	1.528509	3.72807	2.736404	0.902193	1.357018	52.820535	26.599983	137.803582	110.242866	59.187023	27.924121
	5163	0.939474	1.289912	4.592982	3.862281	0.514474	0.589035	33.598601	15.909076	130.800512	104.64041	96.988415	64.401664
	5164	1.08114	1.543421	4.108333	3.131579	0.477193	0.917105	47.890866	23.774947	118.589714	94.871771	74.580482	38.863243
	5166	0.939474	1.014035	4.637719	3.892105	0.260965	0.969298	33.888607	16.077171	104.497831	83.598265	99.215474	65.592732
	5180	1.0625	1.706439	4.475379	3.953788	0.347727	0.341288	25.386983	11.654678	120.296885	96.237508	91.262184	68.093469
	3534	0.820175	0.857456	3.646053	2.870614	0.730702	0.872368	44.015705	21.267903	96.759712	77.40777	56.117074	31.416748
	3535	0.924561	1.237719	4.190351	3.288158	0.924561	1.282456	44.018605	21.530249	154.488415	123.590732	78.152109	43.750641
	3540	0.820175	1.230263	4.369298	3.467105	0.551754	0.842544	42.3518	20.648466	111.436135	89.148908	86.256018	49.725042
Cfast kd + MI	5169	1.006579	1.550877	3.578947	2.244298	0.782895	1.461404	68.25463	37.291667	114.64575	91.7166	53.670932	17.038036
	5170	0.984211	1.476316	3.854825	2.736404	0.663596	0.932018	56.440525	29.013535	115.127142	92.101714	64.105734	27.924121
	5171	1.014035	1.640351	3.549123	2.341228	0.685965	1.357018	63.98113	34.033619	105.220914	84.176731	52.602725	18.946907
	5175	1.02	1.4875	4.030417	2.734167	0.6375	1.1475	60.898419	32.161685	124.829589	99.863671	71.270343	27.867831
	5177	0.94693	1.431579	4.160526	2.669298	0.775439	1.498684	65.822735	35.842295	138.552993	110.842394	76.842963	26.262823
	5178	0.984211	1.342105	3.832456	2.684211	0.827632	1.222807	57.883326	29.961075	130.073582	104.058866	63.222309	26.627134
	3537	0.529386	1.036404	3.899561	2.400877	0.715789	1.088596	69.376679	38.432121	80.947784	64.758227	65.892337	20.178422
	3538	0.669697	0.95303	3.889394	2.826894	0.721212	1.101136	53.799374	27.31788	93.071439	74.457151	65.483979	30.254008
	3539	0.812719	1.334649	4.15307	2.840789	0.61886	0.976754	59.981823	31.597854	107.978434	86.382747	76.517538	30.620924
	3533	0.909649	1.461404	3.899561	2.848246	1.021491	1.215351	53.228485	26.95983	146.290977	117.032782	65.892337	30.818844

Echocardiography examination of cardiac function after *Cfast*-depletion and 4-week of Sham													
Group	**Ear tag**	**IVS;d (mm)**	**IVS;s (mm)**	**LVID;d (mm)**	**LVID;s (mm)**	**LVPW;d (mm)**	**LVPW;s (mm)**	**EF (%)**	**FS (%)**	**LV Mass (mg)**	**LV Mass (Corrected) (mg)**	**LV Vol;d (ul)**	**LV Vol;s (ul)**
Control + Sham	9208	1.040517	1.626724	3.326724	1.67069	0.791379	0.981897	82.181321	49.779723	105.785152	84.628122	45.003066	8.018952
	9204	0.893966	1.450862	2.740517	1.231034	1.011207	1.289655	87.168154	55.080228	83.906025	67.12482	28.027783	3.596482
	9205	0.981897	1.201724	2.637931	1.157759	1.128448	1.568103	88.028739	56.111096	93.399738	74.71979	25.505634	3.053346
***Cfast* kd + Sham**	9203	0.718103	1.143103	2.637931	1.24569	0.87931	1.406897	85.448352	52.777764	60.671408	48.537126	25.505634	3.71149
	9206	0.85	1.289655	2.989655	1.480172	0.967241	1.289655	83.142882	50.490207	88.818117	71.054494	34.705659	5.850374
	9207	0.674138	0.835345	2.799138	1.406897	0.703448	1.157759	82.658998	49.738205	53.630676	42.904541	29.52838	5.120517

Supplemental Table 2 Echocardiography examination of cardiac function after Cfast-depletion and 3-week of isoproterenol injection

Echocardiography examination of cardiac function after *Cfast*-depletion and 3-week of isoproterenol (ISO) injection													
Group	**Ear tag**	**IVS;d**	**IVS;s**	**LVID;d**	**LVID;s**	**LVPW;d**	**LVPW;s**	**EF**	**FS**	**LV Mass**	**LV Mass (Corrected)**	**LV Vol;d**	**LV Vol;s**
Control + ISO	8602	0.676136	0.6375	3.750247	2.938043	0.813043	0.794565	44.600568	21.657347	95.913296	76.730637	60.032316	33.257562
	8603	0.760128	0.913834	3.303409	2.272826	0.804644	0.869318	60.247318	31.19756	83.527583	66.822066	44.243611	17.588022
	8610	0.63666	0.720652	2.842292	1.977174	0.760968	0.794565	59.685993	30.437337	56.081623	44.865298	30.66076	12.360581
	8611	0.734091	0.865119	3.492391	2.328261	0.714773	0.74417	63.075338	33.333324	82.186345	65.749076	50.60286	18.684935
	8612	0.714773	0.714773	3.148864	2.376136	0.579545	0.656818	50.079425	24.539898	59.488849	47.591079	39.387251	19.662342
	8527	0.772727	0.734091	3.651136	2.743182	0.734091	0.540909	50.101803	24.867712	93.245457	74.596366	56.304766	28.095063
***Cfast* kd + ISO**	8601	0.693775	0.826482	3.048913	1.962055	0.560227	0.626581	66.709742	35.647393	54.046809	43.237447	36.410217	12.121055
	8606	0.699654	0.824382	3.687253	2.450469	0.519071	0.882337	63.163663	33.542152	71.550127	57.240102	57.648167	21.235473
	8608	0.52957	0.810524	3.267712	1.794911	0.594664	0.713093	77.608537	45.071322	52.465347	41.972278	43.094474	9.649483
	8614	0.628261	0.729891	3.464674	2.217391	0.628261	0.74837	66.704392	36.00001	67.017316	53.613853	49.641088	16.528302
	8530	0.560227	1.120455	3.825	2.298864	0.560227	0.85	71.239793	39.89898	68.435919	54.748735	62.929315	18.098601
	8531	0.683696	0.572826	3.326087	2.051087	0.628261	0.73913	69.832225	38.333333	66.312722	53.050178	44.982223	13.570136

Supplemental Table 3. Primers used for qRT-PCR

Supplemental Table 3. Primers used for qRT-PCR			
Species	**lncRNA**	**Forward primer sequences**	**Reverse primer sequences**
Mouse	NR-102296	GCGGGAGTAACAAGGACACA	AAAACGGAGCCTGACACCAT
Mouse	NC-000072	CACTTTGCTATGGCACGCTC	AGGCAGATGAAGCAAGGTCC
Mouse	NR-038009	GCTGCGGCAGTTTGTTACTC	TAGCAGATGCTTGGGTGAGC
Mouse	NR-015519	TCTGCAAACTACCTCTGCCG	CCGAAAACCAGGACCAGTCA
Mouse	NR-033498	AGCCCCACATAAGGAACTGC	ACTGCCACTGCACTCTCATC
Mouse	NR-024720	TCACAGCCGAAATCAAAGCAC	TTCACCAAGAAGCATTCGGTTC
Mouse	NC-000071	GGCCTTTTGCTTAGCACTGG	GCTTTGTAAGGCCACGGTTC
Mouse	lncRNA-Cfast	TCCTGGGTTTGGTAACTGCC	GAATTCTGCTGGCCTGAGGT
Human	n338538	AAAATAAACTCTTTGGCTCAGTTTGT	GATCTCCTCGGGGCTCAG
Human	n384785	CAGCTTCTTCTGCATCTGAGG	TGCGGTTAGAAACTCAGCTAGAA
Human	lncRNA-Cfast-1	AGACAGGGGCATTGCCTTTA	CAAGGCTCCCCAGCAGATAA
Human	lncRNA-Cfast-2	TCTTTCCCGATCCAATGTGCT	GTCAATGGCTCCATCTGGCT
Species	**mRNA**	**Forward primer sequences**	**Reverse primer sequences**
Mouse	Nppa	CACAGATCTGATGGATTTCAAGA	CCTCATCTTCTACCGGCATC
Mouse	Nppb	GTCAGTCGTTTGGGCTGTAAC	AGACCCAGGCAGAGTCAGAA
Mouse	Myh7	CGCATCAAGGAGCTCACC	CTGCAGCCGCAGTAGGTT
Mouse	Col1a1	CATGTTCAGCTTTGTGGACCT	GCAGCTGACTTCAGGGATGT
Mouse	Col3a1	TCCCCTGGAATCTGTGAATC	TGAGTCGAATTGGGGAGAAT
Mouse	Fn1	CCTTCCTGTGGCTCCAGA T	GCTGCCCCCATTCATACA
Mouse	Eln	TGGAGCAGGACTTGGAGGT	CCTCCAGCACCATACTTAGCA
Mouse	α-Sma	CCAGCACCATGAAGATCAAG	TCCACATCTGCTGGAAGGTA
Mouse	Cotl1	ACCGACAAGACGCTGGTG	GCTGATCACAAATTCCTTTGC
Mouse	Myh6	GGGCTGGAGCACTGAGAG	GAGAGAGGAACAGGCAGGAA
Mouse	Gapdh	TGCACCACCAACTGCTTAGC	GGCATGGACTGTGGTCATGAG
Mouse	18S RNA	TCCGACCATAAACGATGCCG	CAATCTGTCAATCCTGTCCGTGTC
Mouse	Neat1	TGGCCCCTTTTGTTCATTAGC	TGGAAGGCCATTGTTTCAGG
Mouse	Xist	GGAAAGCCCCAAGTAAAAGG	CCAGGAACCATTCTTGCCTA
Mouse	Postn	AAGCTGCGGCAAGACAAG	TCAAATCTGCAGCTTCAAGG
Human	Nppa	CAGGATGGACAGGATTGGA	TGTCCTCCCTGGCTGTTATC
Human	Nppb	GATGGTGCAAGGGTCTGG	TAATGCCGCCTCAGCACT
Human	β-actin	CCAACCGCGAGAAGATGA	CCAGAGGCGTACAGGGATAG

Supplemental Table 4. Primers used for RACE

Supplemental Table 4. Primers used for RACE	
Primer name	**Primer sequence**
5' RACE-GSP-Cfast	CTGGAAGAGAACACCCTGCTCCC
5' RACE-GSP2-Cfast	GGGAGCAGGGTGTTCTCTTC
3' RACE-GSP-Cfast	GAAACCAGACCATCAGGAGGTAGC
3' RACE-GSP2-Cfast	GCTACCTCCTGATGGTCTGG
Cfast full sequence primer F	CCCATGTACTCTGCGTGGATACC
Cfast full sequence primer R	ATGTCGTATACATACATTTATTGCATGGCTCC

Supplemental Table 5. Sequences for shRNAs and siRNAs

Sequences for shRNAs		
Name	**Sense (5'-3')**	**Antisense (5'-3')**
Control shRNA	GTACGTCGTGAACCCTTGAAGATTAGT	ACTAATCTTCAAGGGTTCACGACGTAC
Cfast shRNA	GTCTGAATGTATCAATGGGCCTAGTCA	TGACTAGGCCCATTGATACATTCAGAC
Sequences for siRNAs		
Name	**Sense (5'-3')**	**Antisense (5'-3')**
Cfast siRNA-1	CCAACAACUUCAUUCACAUTT	AUGUGAAUGAAGUUGUUGGTT
Cfast siRNA-2	CCUGCAUUUGUAUGGCUAATT	UUAGCCAUACAAAUGCAGGTT

Supplemental Table 6. List of the antibodies used in immunofluorescence (IF), western blot (WB), RNA immunoprecipitation (RIP) and Immunoprecipitation (IP)

List of the antibodies used in immunofluorescence (IF), western blot (WB), RNA immunoprecipitation (RIP) and Immunoprecipitation (IP)				
Primary antibodies	**Source**	**Catalog #**	**Origin**	**Application**
COL3A1	Abclonal	A3795	Rabbit	1:1000for WB
Collagen I	Bioss	bs10423R	Rabbit	1:1000for WB
β-ACTIN	CST	4970s	Rabbit	1:2000for WB
COTL1	Abcam	ab235833	Rabbit	1:1000for WB
TGFβRAP1	Abclonal	A14386	Rabbit	1:1000for WB
phospho-Histone H3	Millipore	06-570	Rabbit	1:400 for IF
α-Smooth Muscle Actin-FITC	SIGMA	F3777	Mouse	1:400 for IF
myosin, sarcomere (MHC)	Developmental Studies Hybridoma Bank	MF20	Mouse	5 μg/ml for IF
Monoclonal ANTI-FLAG	SIGMA	F1804	Mouse	RIP and IP
IgG1 Isotype Control	Invitrogen	MA5-14453	Mouse	RIP and IP
Secondary antibodies				
Alexa Fluor® 594 Goat Anti-Rabbit	Invitrogen	A-11012	Goat	1:400 for IF
Alexa Fluor® 488 Goat Anti-Mouse	Invitrogen	A-11001	Goat	1:400 for IF
Alexa Fluor™ 594 Conjugate, Wheat Germ Agglutinin (WGA)	Invitrogen	W11262		1:400 for IF
Goat anti-mouse IgG HRP	Hangzhou Huaan Biotechnology	HA1006	Goat	1:2000for WB
Goat anti-rabbit IgG HRP	Hangzhou Huaan Biotechnology	HA1001	Goat	1:2000for WB